JOURNAL OF SPACECRAFT AND ROCKETS
Vol. 55, No. 5, September–October 2018

Robust Attitude Control Using a Double-Gimbal Variable-Speed Control Moment Gyroscope

Takahiro Sasaki* and Takashi Shimomura†
Osaka Prefecture University, Sakai, Osaka 599-8531, Japan
and
Hanspeter Schaub‡
University of Colorado, Boulder, Colorado 80309

DOI: 10.2514/1.A34120

This paper derives a linear parameter-varying (LPV) model for three-axis attitude control of a spacecraft with a single double-gimbal variable-speed control moment gyroscope (DGVSCMG) and magnetic torquers (MTQs) and develops a singularity avoidance steering law. The LPV control theory provides an optimal gain-scheduled (GS) controller while considering both control performance and robustness. However, in the spacecraft attitude control problem, it is impossible to design a GS controller due to excesses of the number of parameters in most mission scenarios. To avoid this difficulty, this paper designs two types of easy-to-use LPV models for adapting an LPV control theory. The first model is developed by linearization of the kinematics around the equilibrium point of the target attitude. The second one is developed by introducing a virtual state variable together with a parameter-dependent coordinate transformation. Next, a GS controller is designed by using linear matrix inequalities with regional pole placement constraints. Besides, the singularity avoidance steering law of a DGVSCMG by using MTQs is proposed. The applicability is demonstrated through numerical simulations of the proposed methods.

Nomenclature

a	=	semimajor axis, km
$\mathcal{B}$	=	body-fixed frame
$\boldsymbol{b}$	=	geomagnetic field, $\mathrm{N \cdot m^{-1} \cdot A^{-1}}$
$\boldsymbol{H}$	=	total angular momentum, $\mathrm{N \cdot m \cdot s}$
$\boldsymbol{H}_B$	=	angular momentum of the spacecraft excluding a DGVSCMG, $\mathrm{N \cdot m \cdot s}$
$\boldsymbol{H}_{\mathrm{gi}}$, $\boldsymbol{H}_{\mathrm{go}}$	=	angular momentum of the inner/outer gimbal, $\mathrm{N \cdot m \cdot s}$
$\boldsymbol{H}_{\mathrm{ws}}$	=	angular momentum of the wheel, $\mathrm{N \cdot m \cdot s}$
$[I_{\mathrm{gi}}]$, $[I_{\mathrm{go}}]$	=	inertia matrices of inner/outer gimbal axis, $\mathrm{kg \cdot m^2}$
$[I_s]$	=	inertia matrix of the spacecraft including a DGVSCMG as point of masses, $\mathrm{kg \cdot m^2}$
$[I_{\mathrm{ws}}]$	=	inertia matrix of wheel spin axis, $\mathrm{kg \cdot m^2}$
i	=	inclination, rad
$[J]$	=	inertia matrix of the spacecraft including a double-gimbal variable-speed control moment gyroscope (DGVSCMG), $\mathrm{kg \cdot m^2}$
$\boldsymbol{m}_{\mathrm{MTQ}}$	=	magnetic moments, $\mathrm{A \cdot m^2}$
$\mathcal{N}$	=	inertial frame
n	=	orbit rate, rad/s
$\hat{\boldsymbol{s}}$, $\hat{\boldsymbol{g}}_i$, $\hat{\boldsymbol{g}}_o$	=	spin axis, inner gimbal axis, and outer gimbal axis unit vectors of a DGVSCMG
$\mathcal{W}$, $\mathcal{G}_i$, $\mathcal{G}_o$	=	spin axis, inner gimbal axis, and outer gimbal axis frame
$\boldsymbol{\omega}$	=	angular velocity vector of the spacecraft, rad/s
Ω	=	wheel spin rate, rad/s
δ_i, δ_o	=	inner/outer gimbal angle, rad
μ	=	total dipole strength, $\mathrm{Wb \cdot m}$
$\boldsymbol{\beta}$	=	Euler parameters
$\boldsymbol{\sigma}$, $\boldsymbol{\sigma}^S$	=	modified Rodrigues parameters (MRPs), shadow MRPs
$\boldsymbol{\sigma}_e$	=	error MRPs
$\boldsymbol{\rho}$	=	scheduling parameter vector
$\boldsymbol{\tau}_{\mathrm{MTQ}}$	=	MTQ torque vector, $\mathrm{N \cdot m}$
$\boldsymbol{\tau}_d$	=	disturbance torque vector, $\mathrm{N \cdot m}$

Received 19 October 2017; revision received 30 April 2018; accepted for publication 24 May 2018; published online 20 August 2018.

*Graduate Student, Department of Aerospace Engineering, Graduate School of Engineering, Research Fellow of Japan Society for the Promotion of Science, Visiting Scholar at University of Colorado Boulder. Student Member AIAA.

†Professor, Department of Aerospace Engineering, Graduate School of Engineering. Senior Member AIAA.

‡Professor, Glenn L. Murphy Chair of Engineering, Department of Aerospace Engineering Science, Colorado Center for Astrodynamics Research. Associate Fellow AIAA.

I. Introduction

MOMENTUM exchange devices (MEDs) are popular actuators to control the spacecraft attitude as they are electrically actuated and do not require fuel. MEDs consist of control moment gyroscopes (CMGs) and reaction wheels (RWs). The RWs are often used for attitude control of satellites due to their mechanical simplicity, lower cost, and simpler control law algorithms [1,2]. However, RWs cannot respond to the demand of a high-speed attitude maneuver because they cannot provide both a high-speed wheel spin rate and large RW motor torque. The RW electrical power requirement scales with the rotor speed and reaches a limit of available power. Further, there are mechanical limits to how fast a rotor can spin without causing structural issues. In contrast, CMGs are capable of producing large gyroscopic control torques onto the spacecraft that are proportional to the rotor speed and the gimbal rate. The challenges of CMGs are increased mechanical and control algorithm complexity, as well as increased device cost. There are various types of CMGs. Single-gimbal CMGs (SGCMGs) are the most common type of CMG devices. Here the rotor is only able to gimbal about a single-body fixed axes to produce the desired control torque. A particular challenge of an SGCMG cluster is that they cannot always output the desired torque at singular gimbal configurations, often referred to as gimbal lock. Several singularity avoidance methods have been proposed [3–6]. However, they tend to result in complexity of the algorithm and only approximately implement the desired control torque in the neighborhood of the singular configuration.

Single-gimbal variable-speed CMGs (SGVSCMGs) are a hybrid system that consists of an RW and an SGCMG. The extra degree of freedom (DOF) of the wheel spin rate changes enable avoiding the classical SGCMG singularities at the cost of additional power and large rotor speed changes [7–11]. On the other hand, double-gimbal

CMGs (DGCMGs) can apply control torques around arbitrary axes except for singular orientations corresponding to a gimbal lock, where both inner and outer gimbals coincide with each other. To avoid such a gimbal lock, large angular motions should not be commanded in one time [12]. As a practical application, they have been used for international space station (ISS) due to their ability to absorb large amounts of angular momentum. A double-gimbal variable-speed CMG (DGVSCMG) has two gimbal axes and a variable speed wheel. A DGVSCMG can generate large three-dimensional torques if the RW motor torque is sized accordingly. This advantage enables a high-speed attitude maneuver. Some studies related to DGVSCMGs are discussed in Refs. [13–18]. In particular, Stevenson and Schaub [13] develop the spacecraft-DGVSCMG dynamics and presented a nonlinear control algorithm with a Newton–Raphson (NR) scheme. Zhang and Fang [14] apply robust backstepping control while considering disturbance torques to the attitude control problem by using a DGVSCMG. Further, Jikuya et al. [15] show two types of computational procedures for a rest-to-rest maneuver using a DGVSCMG. Sasaki and Shimomura [16] apply postguaranteed convex optimization method to approximated model of the DGVSCMG dynamics. References [17,18] discuss a spacecraft equipped with multiple DGVSCMGs.

Singular device configurations are also a serious challenge in an attitude control of a spacecraft with DGVSCMGs. Multiple DGVSCMGs [17] easily avoid their singularities by using the rotor speed change or null motion as with the singularity avoidance method with VSCMGs [7]. However, with a single DGVSCMG it is difficult to avoid the singularity because it has no redundancy. Reference [15] designs the optimal trajectory of the gimbals and avoids the singularity problem by switching off the feedback compensation near the singularities. Although this approach is practical, it needs a high calculation cost and ignores optimality near the singularities. Reference [14] introduces the terms of the inner gimbal to calculate the actuator input, but it does not guarantee steering the inner gimbal away from the singularity. In addition, previous studies [13,14] conclude that it is preferred to include other attitude actuators to avoid singularities such as one RW or magnetic torquers (MTQs) [19,20]. Based on this insight, this paper studies the singularity avoidance of a DGVSCMG while augmenting the control authority with MTQs.

The satellite dynamics with DGVSCMGs are described through a set of nonlinear differential equations. Most of recent studies about attitude control have used nonlinear controllers such as Lyapunov function-based controllers [21,22]. With Lyapunov function-based controllers, overall stability of attitude control is always guaranteed. However, the closed-loop control performance is not discussed in detail. To study the DGVSCMG performance, the linear parameter-varying (LPV) control theory [23,24] is applied to the attitude control problems [25,26]. In LPV control theory, to avoid difficulties coming from the nonlinearity in satellite dynamics, the dynamics of spacecraft is modeled as an LPV system. A gain-scheduled (GS) controller is applied to this model using linear matrix inequalities (LMIs). However, in the spacecraft attitude control problem, it is impossible to design a GS controller due to excesses of the number of scheduling parameters in most cases. In previous research, Sasaki et al. [25] applies to the stabilization problem (it only controls the angular velocity) of a spacecraft while geometrically considering the operation range of the scheduling parameters. Kwon et al. [26] applies the LPV control theory to the pointing control of a spacecraft and reduces the number of the scheduling parameters by inserting a first-order filter. However, a delay of a phase is generated.

In this study, first of all, two types of new simple LPV models are considered to design the GS controllers for realizing the three-axis attitude control of a spacecraft with a DGVSCMG and MTQs. The first model is studied through linearization of the kinematics around the equilibrium point of the target attitude. The second method is developed by introducing a virtual state variable together with a parameter-dependent coordinate transformation (PDCT). Then, a singularity avoidance steering law of a DGVSCMG by using MTQs is developed. Finally, through numerical simulations, the effectiveness of the proposed GS controller and the proposed singularity avoidance steering law is demonstrated.

II. Spacecraft Model

In this paper, a spacecraft is studied, which has a single DGVSCMG device as modeled in Fig. 1 and three MTQs. This section develops the associated spacecraft dynamics with a DGVSCMG and MTQs. Next, the rigid body kinematic equations are reviewed.

A. Dynamics

The spacecraft considered in this paper is assumed to be a rigid body and contains a single DGVSCMG device and three MTQs. The body-fixed frame $\mathcal{B}$ is represented by a set of unit vectors $\hat{\boldsymbol{x}}_B$, $\hat{\boldsymbol{y}}_B$, and $\hat{\boldsymbol{z}}_B$. The inertial frame is given by $\mathcal{N}$. Then, as in Fig. 2, the unit vectors of the spin axis, the inner gimbal axis, and the outer gimbal axis are denoted by $\hat{\boldsymbol{s}}$, $\hat{\boldsymbol{g}}_i$, and $\hat{\boldsymbol{g}}_o$, respectively. The symbols $\mathcal{G}_o$, $\mathcal{G}_i$, and $\mathcal{W}$ denote the outer gimbal axis frame, the inner gimbal axis frame, and the spin axis frame, respectively. The outer gimbal axis $\hat{\boldsymbol{g}}_o$ is always paralleled to $\hat{\boldsymbol{z}}_B$ of the body frame $\mathcal{B}$. Therefore, it is given by

$$ {}^{\mathcal{G}_o}\hat{\boldsymbol{g}}_o = {}^{\mathcal{G}_o}\begin{bmatrix} 0 \\ 0 \\ 1 \end{bmatrix}, \qquad {}^{\mathcal{B}}\hat{\boldsymbol{g}}_o = {}^{\mathcal{B}}\begin{bmatrix} 0 \\ 0 \\ 1 \end{bmatrix} \tag{1} $$

The inner gimbal axis $\hat{\boldsymbol{g}}_i$ must rotate around the outer gimbal axis $\hat{\boldsymbol{g}}_o$. Therefore, it is given as follows:

$$ {}^{\mathcal{G}_i}\hat{\boldsymbol{g}}_i = {}^{\mathcal{G}_i}\begin{bmatrix} 0 \\ 1 \\ 0 \end{bmatrix}, \quad {}^{\mathcal{G}_o}\hat{\boldsymbol{g}}_i = {}^{\mathcal{G}_o}\begin{bmatrix} -\sin\delta_o \\ \cos\delta_o \\ 0 \end{bmatrix}, \quad {}^{\mathcal{B}}\hat{\boldsymbol{g}}_i = {}^{\mathcal{B}}\begin{bmatrix} -\sin\delta_o \\ \cos\delta_o \\ 0 \end{bmatrix} \tag{2} $$

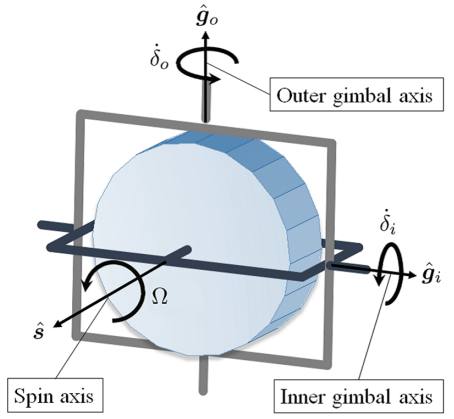

Fig. 1 DGVSCMG frame and axes illustration.

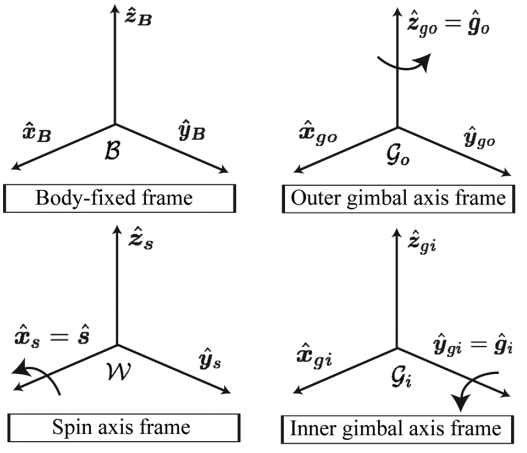

Fig. 2 Definition of DGVSCMG's frame.

where δ_o is the outer gimbal angle. The spin axis $\hat{\boldsymbol{s}}$ can be expressed as follows:

$$
{}^{\mathcal{W}}\hat{\boldsymbol{s}} = {}^{\mathcal{W}}\begin{bmatrix} 1 \\ 0 \\ 0 \end{bmatrix}, \qquad {}^{\mathcal{G}_i}\hat{\boldsymbol{s}} = {}^{\mathcal{G}_i}\begin{bmatrix} \cos\delta_i \\ 0 \\ -\sin\delta_i \end{bmatrix},
$$
$$
{}^{\mathcal{G}_o}\hat{\boldsymbol{s}} = {}^{\mathcal{G}_o}\begin{bmatrix} \cos\delta_o\cos\delta_i \\ \sin\delta_o\cos\delta_i \\ -\sin\delta_i \end{bmatrix}, \qquad {}^{\mathcal{B}}\hat{\boldsymbol{s}} = {}^{\mathcal{B}}\begin{bmatrix} \cos\delta_o\cos\delta_i \\ \sin\delta_o\cos\delta_i \\ -\sin\delta_i \end{bmatrix} \tag{3}
$$

where δ_i is the inner gimbal angle. Next, the dynamics of a spacecraft with a DGVSCMG and MTQs is considered to be expanded on a spacecraft with single DGVSCMG in Ref. [13]. The total inertial angular momentum $\boldsymbol{H}$ is described by

$$
\boldsymbol{H} = \boldsymbol{H}_B + \boldsymbol{H}_{\text{go}} + \boldsymbol{H}_{\text{gi}} + \boldsymbol{H}_{\text{ws}} \tag{4}
$$

together with

$$
\boldsymbol{H}_B = [I_s]\boldsymbol{\omega}_{\mathcal{B}/\mathcal{N}} \tag{5a}
$$

$$
\boldsymbol{H}_{\text{go}} = [I_{\text{go}}]\boldsymbol{\omega}_{\mathcal{G}_o/\mathcal{N}} \tag{5b}
$$

$$
\boldsymbol{H}_{\text{gi}} = [I_{\text{gi}}]\boldsymbol{\omega}_{\mathcal{G}_i/\mathcal{N}} \tag{5c}
$$

$$
\boldsymbol{H}_{\text{ws}} = [I_{\text{ws}}]\boldsymbol{\omega}_{\mathcal{W}/\mathcal{N}} \tag{5d}
$$

where

$$
\boldsymbol{\omega}_{\mathcal{G}_o/\mathcal{N}} = \boldsymbol{\omega}_{\mathcal{B}/\mathcal{N}} + \dot{\delta}_o\hat{\boldsymbol{g}}_o \tag{6a}
$$

$$
\boldsymbol{\omega}_{\mathcal{G}_i/\mathcal{N}} = \boldsymbol{\omega}_{\mathcal{B}/\mathcal{N}} + \dot{\delta}_o\hat{\boldsymbol{g}}_o + \dot{\delta}_i\hat{\boldsymbol{g}}_i \tag{6b}
$$

$$
\boldsymbol{\omega}_{\mathcal{W}/\mathcal{N}} = \boldsymbol{\omega}_{\mathcal{B}/\mathcal{N}} + \dot{\delta}_o\hat{\boldsymbol{g}}_o + \dot{\delta}_i\hat{\boldsymbol{g}}_i + \Omega\hat{\boldsymbol{s}} \tag{6c}
$$

and $[I_s]$ is the inertia matrix of a spacecraft (including the DGVSCMG as point masses) about the overall spacecraft center of mass, $\boldsymbol{\omega}_{\mathcal{B}/\mathcal{N}}$ is the inertial angular velocity of the spacecraft, and $\boldsymbol{\omega}_{\mathcal{G}_o/\mathcal{N}}$, $\boldsymbol{\omega}_{\mathcal{G}_i/\mathcal{N}}$, and $\boldsymbol{\omega}_{\mathcal{W}/\mathcal{N}}$ denote the inertia angular velocity of the outer gimbal, inner gimbal, and wheel, respectively. $[I_{\text{gi}}]$ or $[I_{\text{go}}]$ is the moment of inertia matrix of the DGVSCMG about the inner or outer gimbal axis, respectively; $[I_{\text{ws}}]$ is the moment of inertia matrix of the wheel about the spin axis; and Ω is the wheel spin rate. The total inertia matrix $[J]$ of a spacecraft including a DGVSCMG device is given by

$$
[J] = [I_s] + [I_{\text{go}}] + [I_{\text{gi}}] + [I_{\text{ws}}] \tag{7}
$$

This inertia tensor $[J]$ will vary with time as seen by the body frame. Note that ${}^{\mathcal{B}}[I_s]$, ${}^{\mathcal{G}_o}[I_{\text{go}}]$, ${}^{\mathcal{G}_i}[I_{\text{gi}}]$, and ${}^{\mathcal{G}_i}[I_{\text{ws}}]$ are constant matrices. The dynamics of a spacecraft with a DGVSCMG and MTQs is given by

$$
\dot{\boldsymbol{H}} = \boldsymbol{\tau}_{\text{MTQ}} + \boldsymbol{\tau}_d \tag{8}
$$

where the vector $\boldsymbol{\tau}_{\text{MTQ}}$ denotes the external torque by the MTQs and $\boldsymbol{\tau}_d$ represents the sum of all the external torques experienced by the spacecraft. Substituting Eq. (4) into Eq. (8) yields

$$
\dot{\boldsymbol{H}}_B + \dot{\boldsymbol{H}}_{\text{go}} + \dot{\boldsymbol{H}}_{\text{gi}} + \dot{\boldsymbol{H}}_{\text{ws}} = \boldsymbol{\tau}_{\text{MTQ}} + \boldsymbol{\tau}_d \tag{9}
$$

In the following development, the short-hand notations $\boldsymbol{\omega} = \boldsymbol{\omega}_{\mathcal{B}/\mathcal{N}}$, $\boldsymbol{\omega}_{\text{go}} = \boldsymbol{\omega}_{\mathcal{G}_o/\mathcal{N}}$, $\boldsymbol{\omega}_{\text{gi}} = \boldsymbol{\omega}_{\mathcal{G}_i/\mathcal{N}}$, and $\boldsymbol{\omega}_{\text{ws}} = \boldsymbol{\omega}_{\mathcal{W}/\mathcal{N}}$ are used to make equation description more compact. Taking the inertial time derivative of the first term of the LHS in Eq. (9) leads to

$$
\dot{\boldsymbol{H}}_B = [I_s]\dot{\boldsymbol{\omega}} + \boldsymbol{\omega}^{\times}[I_s]\boldsymbol{\omega} \tag{10}
$$

Note that the notation $\boldsymbol{x}^{\times}$ denotes the following skew-symmetric matrix:

$$
\boldsymbol{x}^{\times} := \begin{bmatrix} 0 & -x_3 & x_2 \\ x_3 & 0 & -x_1 \\ -x_2 & x_1 & 0 \end{bmatrix}, \qquad {}^{\forall}\boldsymbol{x} = [\,x_1 \quad x_2 \quad x_3\,]^T \tag{11}
$$

The second term of the LHS in Eq. (9) is related to the outer gimbal of the DGVSCMG. This is shown as follows:

$$
\dot{\boldsymbol{H}}_{\text{go}} = [I_{\text{go}}]\Big(\dot{\boldsymbol{\omega}} + \ddot{\delta}_o\hat{\boldsymbol{g}}_o + \boldsymbol{\omega}^{\times}(\dot{\delta}_o\hat{\boldsymbol{g}}_o)\Big) + \boldsymbol{\omega}_{\text{go}}^{\times}([I_{\text{go}}]\boldsymbol{\omega}_{\text{go}}) \tag{12}
$$

The third term of the LHS in Eq. (9) is related to the inner gimbal of the DGVSCMG. This is shown as follows:

$$
\begin{aligned}
\dot{\boldsymbol{H}}_{\text{gi}} = {} & [I_{\text{gi}}]\Big(\dot{\boldsymbol{\omega}} + \ddot{\delta}_o\hat{\boldsymbol{g}}_o + \ddot{\delta}_i\hat{\boldsymbol{g}}_i + \boldsymbol{\omega}^{\times}(\dot{\delta}_o\hat{\boldsymbol{g}}_o + \dot{\delta}_i\hat{\boldsymbol{g}}_i) + (\dot{\delta}_o\hat{\boldsymbol{g}}_o)^{\times}(\dot{\delta}_i\hat{\boldsymbol{g}}_i)\Big) \\
& + \boldsymbol{\omega}_{\text{gi}}^{\times}([I_{\text{gi}}]\boldsymbol{\omega}_{\text{gi}})
\end{aligned} \tag{13}
$$

The fourth term of the LHS in Eq. (9) is related to the wheel spin rate of the DGVSCMG. This is shown as follows:

$$
\begin{aligned}
\dot{\boldsymbol{H}}_{\text{ws}} = {} & [I_{\text{ws}}]\Big(\dot{\omega} + \ddot{\delta}_o\hat{\boldsymbol{g}}_o + \ddot{\delta}_i\hat{\boldsymbol{g}}_i + \dot{\Omega}\,\hat{\boldsymbol{s}} + \omega^{\times}(\dot{\delta}_o\hat{\boldsymbol{g}}_o + \dot{\delta}_i\hat{\boldsymbol{g}}_i + \Omega\hat{\boldsymbol{s}}) \\
& + (\dot{\delta}_o\hat{\boldsymbol{g}}_o)^{\times}(\dot{\delta}_i\hat{\boldsymbol{g}}_i + \Omega\hat{\boldsymbol{s}}) + (\dot{\delta}_i\hat{\boldsymbol{g}}_i)^{\times}(\Omega\hat{\boldsymbol{s}})\Big) + \boldsymbol{\omega}_{\text{ws}}^{\times}([I_{\text{ws}}]\boldsymbol{\omega}_{\text{ws}})
\end{aligned} \tag{14}
$$

The first term of the RHS in Eq. (9) is related to MTQs [19,20]. This is shown as follows:

$$
\boldsymbol{\tau}_{\text{MTQ}} = \boldsymbol{m}_{\text{MTQ}} \times \boldsymbol{b}(t) = -\boldsymbol{b}^{\times}(t)\boldsymbol{m}_{\text{MTQ}} \tag{15}
$$

where the vector $\boldsymbol{m}_{\text{MTQ}} \in R^3$ is the magnetic moments for the three coils, and $\boldsymbol{b}(t)$ is the geomagnetic field at the spacecraft as seen by the inertial frame $\mathcal{N}$. Note that the MTQs are set toward the unit vectors of $\mathcal{B}$. The simplified magnetic model [27] is given by

$$
{}^{\mathcal{N}}\boldsymbol{b}(t) = \begin{bmatrix} b_1(t) \\ b_2 \\ b_3(t) \end{bmatrix} = \frac{\mu}{a^3}\begin{bmatrix} \sin i\cos nt \\ -\cos i \\ 2\sin i\sin nt \end{bmatrix} \tag{16}
$$

where μ is the total dipole strength, a is the semimajor axis, i is the inclination, and n is the orbit rate. In Eq. (16), the time is measured from the point of magnetic equator crossing on the ascending node ($t = 0$). In summary, Eq. (9) is rewritten as the final kinetic equations of motion of a spacecraft with a DGVSCMG and MTQs:

$$
\begin{aligned}
[J]\dot{\boldsymbol{\omega}} = {} & -\boldsymbol{\omega}^{\times}[I_s]\boldsymbol{\omega} - [I_{\text{go}}]\ddot{\delta}_o\hat{\boldsymbol{g}}_o - [I_{\text{go}}]\boldsymbol{\omega}^{\times}(\dot{\delta}_o\hat{\boldsymbol{g}}_o) - \boldsymbol{\omega}_{\text{go}}^{\times}([I_{\text{go}}]\boldsymbol{\omega}_{\text{go}}) \\
& - [I_{\text{gi}}]\ddot{\delta}_o\hat{\boldsymbol{g}}_o - [I_{\text{gi}}]\ddot{\delta}_i\hat{\boldsymbol{g}}_i - [I_{\text{gi}}]\boldsymbol{\omega}^{\times}(\dot{\delta}_o\hat{\boldsymbol{g}}_o) - [I_{\text{gi}}]\boldsymbol{\omega}^{\times}(\dot{\delta}_i\hat{\boldsymbol{g}}_i) \\
& - [I_{\text{gi}}](\dot{\delta}_o\hat{\boldsymbol{g}}_o)^{\times}(\dot{\delta}_i\hat{\boldsymbol{g}}_i) - \boldsymbol{\omega}_{\text{gi}}^{\times}([I_{\text{gi}}]\boldsymbol{\omega}_{\text{gi}}) - [I_{\text{ws}}]\ddot{\delta}_o\hat{\boldsymbol{g}}_o - [I_{\text{ws}}]\ddot{\delta}_i\hat{\boldsymbol{g}}_i \\
& - [I_{\text{ws}}]\dot{\Omega}\,\hat{\boldsymbol{s}} - [I_{\text{ws}}]\boldsymbol{\omega}^{\times}(\dot{\delta}_o\hat{\boldsymbol{g}}_o) - [I_{\text{ws}}]\boldsymbol{\omega}^{\times}(\dot{\delta}_i\hat{\boldsymbol{g}}_i) - [I_{\text{ws}}]\boldsymbol{\omega}^{\times}(\Omega\hat{\boldsymbol{s}}) \\
& - [I_{\text{ws}}](\dot{\delta}_o\hat{\boldsymbol{g}}_o)^{\times}(\dot{\delta}_i\hat{\boldsymbol{g}}_i) - [I_{\text{ws}}](\dot{\delta}_o\hat{\boldsymbol{g}}_o)^{\times}(\Omega\hat{\boldsymbol{s}}) - [I_{\text{ws}}](\dot{\delta}_i\hat{\boldsymbol{g}}_i)^{\times}(\Omega\hat{\boldsymbol{s}}) \\
& - \boldsymbol{\omega}_{\text{ws}}^{\times}([I_{\text{ws}}]\boldsymbol{\omega}_{\text{ws}}) - \boldsymbol{b}^{\times}(t)\boldsymbol{m}_{\text{MTQ}} + \boldsymbol{\tau}_d
\end{aligned} \tag{17}
$$

B. Rigid Body Kinematics

Spacecraft attitude is given by the orientation of the body-fixed frame $\mathcal{B}$ with respect to the inertial frame $\mathcal{N}$. It is known that three kinematic parameters are enough to describe the attitude. As such parameters, in this paper, modified Rodrigues parameters (MRPs) are chosen [28,29]. However, the following development is not tied to this particular choice in attitude coordinates. Other attitude parameterizations could readily be applied. The MRP vector $\boldsymbol{\sigma}$ is defined in terms of the Euler parameters (EPs) $\boldsymbol{\beta}$ as the transformation

$$\sigma_i = \frac{\beta_i}{1+\beta_0} \qquad i = 1,2,3 \tag{18}$$

Note that β_0 and β_i denote the scalar part and the vector one of the EPs, respectively. Using the principal rotation axis vector $\hat{\boldsymbol{e}}$ and the rotation angle Φ, the MRPs are given by

$$\boldsymbol{\sigma} = \tan\left(\frac{\Phi}{4}\right)\hat{\boldsymbol{e}} \tag{19}$$

For such the MRPs, the singular points are given at $\Phi = \pm 2\pi$. When a spacecraft is thrown off by a launch vehicle, there is no guarantee that the kinematic singularity is avoided even when the control objective is set-point regulation as opposed to tracking. However, these singularities can be avoided by introducing the dual-MRP method that consists of the classical MRP and the shadow MRP [28,29]. To introduce the alternate EPs vector $-\boldsymbol{\beta}$, the shadow MRPs and one of the switch surface between these two MRP vectors are defined as follows:

$$\sigma_i^S = -\frac{\beta_i}{1-\beta_0} = -\sigma_i/\sigma^2 \qquad i = 1,2,3 \tag{20}$$

where $\sigma^2 = \boldsymbol{\sigma}^T\boldsymbol{\sigma}$. The shadow MRPs are given by

$$\boldsymbol{\sigma}^S = \tan\left(\frac{\Phi - 2\pi}{4}\right)\hat{\boldsymbol{e}} \tag{21}$$

For such shadow MRPs, the singular points are given at $\Phi = 0$ as compared with the classical MRPs, which are singular at $\Phi = \pm 2\pi$. This allows one to avoid MRP singularities altogether by switching between classical and shadow MRP sets as one MRP vector approaches a singular orientation. The combined set of classical and shadow MRPs with the switching surface $\sigma^2 = 1$ provides for a nonsingular, bounded, minimal attitude description. The original kinematic equation based on the error MRPs $\boldsymbol{\sigma}_e$ and the error angular velocity $\boldsymbol{\omega}_e$ is given by

$$\dot{\boldsymbol{\sigma}}_e = \frac{1}{4}\boldsymbol{H}(\boldsymbol{\sigma}_e)\boldsymbol{\omega}_e \tag{22a}$$

$$\boldsymbol{H}(\boldsymbol{\sigma}_e) = \left[(1-\boldsymbol{\sigma}_e^T\boldsymbol{\sigma}_e)I_3 + 2\boldsymbol{\sigma}_e^{\times} + 2\boldsymbol{\sigma}_e\boldsymbol{\sigma}_e^T\right] \tag{22b}$$

Note that the inverse of $\boldsymbol{H}(\boldsymbol{\sigma}_e)$ is given by

$$\boldsymbol{H}^{-1}(\boldsymbol{\sigma}_e) = \frac{1}{(1+\sigma_e^2)}\boldsymbol{H}^T(\boldsymbol{\sigma}_e), \qquad \sigma_e^2 = \boldsymbol{\sigma}_e^T\boldsymbol{\sigma}_e \tag{23}$$

The direct mapping between the two trajectories $\dot{\boldsymbol{\sigma}}_e$ and $\dot{\boldsymbol{\sigma}}_e^S$ is given by [30]

$$\dot{\boldsymbol{\sigma}}_e^S = -\frac{\dot{\boldsymbol{\sigma}}_e}{\sigma_e^2} + \frac{1}{2}\left(\frac{1+\sigma_e^2}{\sigma_e^4}\right)\boldsymbol{\sigma}_e\boldsymbol{\sigma}_e^T\boldsymbol{\omega}_e \tag{24}$$

as a mapping exists between $\boldsymbol{\sigma}_e$ and $\boldsymbol{\sigma}_e^S$.

III. LPV Modeling

A. LPV Model for Three-Axis Attitude Control

This section investigates the LPV model to design the GS controller for three-axis attitude control. First, Eq. (17) must be transformed into an LPV model that linearly depends on scheduling parameters [23]. To realize the attitude control of a spacecraft, the error angular velocity of a spacecraft $\boldsymbol{\omega}_e$ is considered as the state feedback variable, and the DGVSCMG input $\dot{\Omega}$, $\dot{\delta}_i$, $\dot{\delta}_o$ and the MTQs input $\boldsymbol{m}_{\mathrm{MTQ}}$ are considered as the control input of the plant. The Jacobian linearization of Eq. (17) around the equilibrium point ($\boldsymbol{\omega}_{e,\mathrm{eq}} = \boldsymbol{0}, \dot{\Omega}_{\mathrm{eq}} = 0, \dot{\delta}_{i,\mathrm{eq}} = 0, \dot{\delta}_{o,\mathrm{eq}} = 0, \boldsymbol{m}_{\mathrm{MTQ,eq}} = \boldsymbol{0}$) leads to the linear dynamics of a spacecraft with a DGVSCMG and MTQs. The spacecraft dynamics and the kinematics equations based on the MRPs are given as follows:

$$\dot{\boldsymbol{\omega}}_e = \boldsymbol{A}(\boldsymbol{\rho})\boldsymbol{\omega}_e + \boldsymbol{B}_1(\boldsymbol{\rho})\boldsymbol{u}_{\mathrm{DGV}} + \boldsymbol{B}_2(\boldsymbol{\rho})\boldsymbol{m}_{\mathrm{MTQ}} + \boldsymbol{E}w \tag{25}$$

$$\dot{\boldsymbol{\sigma}}_e = \frac{1}{4}\boldsymbol{H}(\boldsymbol{\sigma}_e)\boldsymbol{\omega}_e \tag{26}$$

where $\boldsymbol{u}_{\mathrm{DGV}} = [\,\dot{\Omega} \quad \dot{\delta}_i \quad \dot{\delta}_o\,]^T$ is the DGVSCMG control input, $\boldsymbol{E}w$ the disturbance term including model errors, and the coefficient matrices are given as follows:

$$\boldsymbol{A}(\boldsymbol{\rho}) = [J]^{-1}[I_{\mathrm{ws}}]\boldsymbol{M}(\boldsymbol{\rho}) \tag{27}$$

$$\boldsymbol{B}_1(\boldsymbol{\rho}) = \bar{\boldsymbol{B}}_1\boldsymbol{N}_1(\boldsymbol{\rho}), \qquad \bar{\boldsymbol{B}}_1 = -[J]^{-1}[I_{\mathrm{ws}}] \tag{28}$$

$$\boldsymbol{B}_2(\boldsymbol{\rho}) = \bar{\boldsymbol{B}}_2\boldsymbol{N}_2(\boldsymbol{\rho}), \qquad \bar{\boldsymbol{B}}_2 = [J]^{-1}\frac{\mu}{a^3} \tag{29}$$

with

$$\boldsymbol{M}(\boldsymbol{\rho}) = (\Omega\hat{\boldsymbol{s}})^{\times} = \begin{bmatrix} 0 & \Omega\sin\delta_i & \Omega\cos\delta_i\sin\delta_o \\ -\Omega\sin\delta_i & 0 & -\Omega\cos\delta_i\cos\delta_o \\ -\Omega\cos\delta_i\sin\delta_o & \Omega\cos\delta_i\cos\delta_o & 0 \end{bmatrix} \tag{30}$$

$$\boldsymbol{N}_1(\boldsymbol{\rho}) = [\,\hat{\boldsymbol{s}} \quad \Omega\hat{\boldsymbol{g}}_i\times\hat{\boldsymbol{s}} \quad \Omega\hat{\boldsymbol{g}}_o\times\hat{\boldsymbol{s}}\,] = \begin{bmatrix} \cos\delta_i\cos\delta_o & -\Omega\sin\delta_i\cos\delta_o & -\Omega\cos\delta_i\sin\delta_o \\ \cos\delta_i\sin\delta_o & -\Omega\sin\delta_i\sin\delta_o & \Omega\cos\delta_i\cos\delta_o \\ -\sin\delta_i & -\Omega\cos\delta_i & 0 \end{bmatrix} \tag{31}$$

$$\boldsymbol{N}_2(\boldsymbol{\rho}) = \begin{bmatrix} 0 & -2\sin i\sin nt & -\cos i \\ 2\sin i\sin nt & 0 & -\sin i\cos nt \\ \cos i & \sin i\cos nt & 0 \end{bmatrix} \tag{32}$$

where $\boldsymbol{\rho}$ and $\boldsymbol{\sigma}_e$ are the scheduling parameter vectors. If $\boldsymbol{\rho}$ is defined by

$$\boldsymbol{\rho} = [\,\Omega \quad \sin\delta_i \quad \cos\delta_i \quad \sin\delta_o \quad \cos\delta_o \quad \sin nt \quad \cos nt\,]^T$$

with $\boldsymbol{\sigma}_e = [\,\sigma_{e1} \quad \sigma_{e2} \quad \sigma_{e3}\,]^T$, this system has 10 scheduling parameters and it is covered with a convex hull that has $2^{10}(=1024)$ extreme points or vertices [23–26] constructed by the combination of the maximum and the minimum values of the scheduling parameters. In LPV control theory, the number of the vertices of the convex hull is equivalent to the number of the LMIs to be solved for control design. These LMIs should be solved simultaneously to guarantee overall stability for a whole operating range. In this way, the scheduling parameters of the LPV model in Eq. (25) have too many vertices to perform the GS controller design. This is the main challenge to adapt the LPV control theory to the spacecraft attitude control problem. To overcome this challenge, several methods are considered to reduce the number of vertices. First, the part that depends on the scheduling parameters of the coefficient matrices $\boldsymbol{B}_1(\boldsymbol{\rho})$ and $\boldsymbol{B}_2(\boldsymbol{\rho})$ are embedded into a virtual control input $\boldsymbol{u}' \in R^3$ as follows:

$$\boldsymbol{u}' = \boldsymbol{N}_1(\boldsymbol{\rho})\boldsymbol{u}_{\mathrm{DGV}} + \bar{\boldsymbol{B}}_1^{-1}\bar{\boldsymbol{B}}_2\boldsymbol{N}_2(\boldsymbol{\rho})\boldsymbol{m}_{\mathrm{MTQ}} \tag{33}$$

where $\bar{\boldsymbol{B}}_1^{-1}$ can always be solved, since $\mathrm{rank}(\bar{\boldsymbol{B}}_1) = 3$. Note that Eq. (33) represents the relationship between the output torque and the set of the gimbal rate and the MTQ magnetic moment. In the case of CMGs, it has a singularity problem. In this paper, this singular configuration challenges are avoided by the use of MTQs' torques.

The detail is discussed later in Sec. V. By using this virtual control input and setting the state variable to $\boldsymbol{x} := [\boldsymbol{\omega}_e^T \quad \boldsymbol{\sigma}_e^T]^T$ for three-axis attitude control, the state-space representation of Eqs. (25) and (26) is given as follows:

$$\begin{bmatrix} \dot{\boldsymbol{\omega}}_e \\ \dot{\boldsymbol{\sigma}}_e \end{bmatrix} = \begin{bmatrix} \boldsymbol{A}(\boldsymbol{\rho}) & \boldsymbol{0} \\ \frac{1}{4}\boldsymbol{H}(\boldsymbol{\sigma}_e) & \boldsymbol{0} \end{bmatrix} \begin{bmatrix} \boldsymbol{\omega}_e \\ \boldsymbol{\sigma}_e \end{bmatrix} + \begin{bmatrix} \bar{\boldsymbol{B}}_1 \\ \boldsymbol{0} \end{bmatrix} \boldsymbol{u}' + \begin{bmatrix} \boldsymbol{E} \\ \boldsymbol{0} \end{bmatrix} \boldsymbol{w} \tag{34}$$

which is equivalently written in a more compact form as

$$\dot{\boldsymbol{x}} = \boldsymbol{A}_e(\boldsymbol{\rho}, \boldsymbol{\sigma}_e)\boldsymbol{x} + \boldsymbol{B}_e\boldsymbol{u}' + \boldsymbol{E}_e\boldsymbol{w} \tag{35}$$

where the coefficient matrices are given by

$$\boldsymbol{A}_e(\boldsymbol{\rho}, \boldsymbol{\sigma}_e) := \begin{bmatrix} \boldsymbol{A}(\boldsymbol{\rho}) & \boldsymbol{0} \\ \frac{1}{4}\boldsymbol{H}(\boldsymbol{\sigma}_e) & \boldsymbol{0} \end{bmatrix}, \quad \boldsymbol{B}_e := \begin{bmatrix} \bar{\boldsymbol{B}}_1 \\ \boldsymbol{0} \end{bmatrix}, \quad \boldsymbol{E}_e := \begin{bmatrix} \boldsymbol{E} \\ \boldsymbol{0} \end{bmatrix} \tag{36}$$

and from Eq. (30), the scheduling parameter vector $\boldsymbol{\rho}$ is given by

$$\boldsymbol{\rho} = \begin{bmatrix} \rho_1 \\ \rho_2 \\ \rho_3 \end{bmatrix} = \begin{bmatrix} \Omega \cos\delta_i \cos\delta_o \\ \Omega \cos\delta_i \sin\delta_o \\ \Omega \sin\delta_i \end{bmatrix} \tag{37}$$

In this way, the number of scheduling parameters in the vectors $\boldsymbol{\rho}$ and $\boldsymbol{\sigma}_e$ is reduced into 6 that yields $64(= 2^6)$ vertices or LMIs. However, it is still too many to design the GS controller. To avoid this situation, from the next subsection, two types of easy-to-use LPV models that have few vertices are investigated.

B. Simple LPV Model (Method 1)

To eliminate the scheduling parameter vector $\boldsymbol{\sigma}_e$ in Eq. (35), the Jacobian linearization of Eq. (22b) around the equilibrium point ($\boldsymbol{\sigma}_{e,\mathrm{eq}} = \boldsymbol{0}$) leads to the linear kinematics as follows:

$$\boldsymbol{H}(\boldsymbol{\sigma}_e) \simeq \boldsymbol{I}_3 \tag{38}$$

Substituting Eq. (38) into Eq. (34), a simple LPV model is given as follows:

$$\begin{bmatrix} \dot{\boldsymbol{\omega}}_e \\ \dot{\boldsymbol{\sigma}}_e \end{bmatrix} = \begin{bmatrix} \boldsymbol{A}(\boldsymbol{\rho}) & \boldsymbol{0} \\ \frac{1}{4}\boldsymbol{I}_3 & \boldsymbol{0} \end{bmatrix} \begin{bmatrix} \boldsymbol{\omega}_e \\ \boldsymbol{\sigma}_e \end{bmatrix} + \begin{bmatrix} \bar{\boldsymbol{B}}_1 \\ \boldsymbol{0} \end{bmatrix} \boldsymbol{u}' + \begin{bmatrix} \boldsymbol{E} \\ \boldsymbol{0} \end{bmatrix} \boldsymbol{w} \tag{39}$$

which is written compactly as

$$\dot{\boldsymbol{x}} = \tilde{\boldsymbol{A}}_e(\boldsymbol{\rho})\boldsymbol{x} + \boldsymbol{B}_e\boldsymbol{u}' + \boldsymbol{E}_e\boldsymbol{w} \tag{40}$$

where

$$\tilde{\boldsymbol{A}}_e(\boldsymbol{\rho}) := \begin{bmatrix} \boldsymbol{A}(\boldsymbol{\rho}) & \boldsymbol{0} \\ \frac{1}{4}\boldsymbol{I}_3 & \boldsymbol{0} \end{bmatrix}, \quad \boldsymbol{B}_e := \begin{bmatrix} \bar{\boldsymbol{B}}_1 \\ \boldsymbol{0} \end{bmatrix}, \quad \boldsymbol{E}_e := \begin{bmatrix} \boldsymbol{E} \\ \boldsymbol{0} \end{bmatrix} \tag{41}$$

The GS controller for this simple LPV model is given by

$$\boldsymbol{u}' = -\boldsymbol{K}(\boldsymbol{\rho})\boldsymbol{x} \tag{42}$$

which allows for simultaneous consideration of overall stability and control performance. In this case, the number of scheduling parameters is reduced into 3, which yields $8(= 2^3)$ vertices, and the GS controller can be easily designed. The GS controller gain $\boldsymbol{K}(\boldsymbol{\rho})$ is designed later in Sec. IV.

C. Simple LPV Model (Method 2)

This section presents the method to reduce the scheduling parameters by using the proposed coordinate transformation and analyze the singularity of the inverse transformation matrix.

1. Parameter-Dependent Coordinate Transformation

To eliminate the scheduling parameter vector $\boldsymbol{\sigma}_e$ in Eq. (35), the second method is presented. By using the parameter-dependent coordinate transformation (PDCT) matrix:

$$\boldsymbol{T}(\boldsymbol{\sigma}_e) := \begin{bmatrix} \boldsymbol{I}_3 & \boldsymbol{0} \\ \boldsymbol{0} & \boldsymbol{H}^{-1}(\boldsymbol{\sigma}_e) \end{bmatrix} \tag{43}$$

the following simple LPV model is obtained, which is easy to use for control design. By using this matrix $\boldsymbol{T}$, Eq. (35) can be expressed as follows:

$$\begin{aligned} \boldsymbol{T}(\boldsymbol{\sigma}_e) \begin{bmatrix} \dot{\boldsymbol{\omega}}_e \\ \dot{\boldsymbol{\sigma}}_e \end{bmatrix} &= \boldsymbol{T}(\boldsymbol{\sigma}_e) \begin{bmatrix} \boldsymbol{A}(\boldsymbol{\rho}) & \boldsymbol{0} \\ \frac{1}{4}\boldsymbol{H}(\boldsymbol{\sigma}_e) & \boldsymbol{0} \end{bmatrix} \boldsymbol{T}^{-1}(\boldsymbol{\sigma}_e)\boldsymbol{T}(\boldsymbol{\sigma}_e) \begin{bmatrix} \boldsymbol{\omega}_e \\ \boldsymbol{\sigma}_e \end{bmatrix} \\ &\quad + \boldsymbol{T}(\boldsymbol{\sigma}_e) \begin{bmatrix} \bar{\boldsymbol{B}}_1 \\ \boldsymbol{0} \end{bmatrix} \boldsymbol{u}' + \boldsymbol{T}(\boldsymbol{\sigma}_e) \begin{bmatrix} \boldsymbol{E} \\ \boldsymbol{0} \end{bmatrix} \boldsymbol{w} \end{aligned} \tag{44}$$

$$\begin{bmatrix} \dot{\boldsymbol{\omega}}_e \\ \boldsymbol{H}^{-1}(\boldsymbol{\sigma}_e)\dot{\boldsymbol{\sigma}}_e \end{bmatrix} = \begin{bmatrix} \boldsymbol{A}(\boldsymbol{\rho}) & \boldsymbol{0} \\ \frac{1}{4}\boldsymbol{I}_3 & \boldsymbol{0} \end{bmatrix} \begin{bmatrix} \boldsymbol{\omega}_e \\ \boldsymbol{H}^{-1}(\boldsymbol{\sigma}_e)\boldsymbol{\sigma}_e \end{bmatrix} + \begin{bmatrix} \bar{\boldsymbol{B}}_1 \\ \boldsymbol{0} \end{bmatrix} \boldsymbol{u}' + \begin{bmatrix} \boldsymbol{E} \\ \boldsymbol{0} \end{bmatrix} \boldsymbol{w} \tag{45}$$

By introducing the following virtual state

$$\boldsymbol{\zeta} = \boldsymbol{H}^{-1}(\boldsymbol{\sigma}_e)\sigma_e \tag{46}$$

$$\dot{\boldsymbol{\zeta}} = \boldsymbol{H}^{-1}(\boldsymbol{\sigma}_e)\dot{\boldsymbol{\sigma}}_e + \frac{\mathrm{d}}{\mathrm{d}t}\{\boldsymbol{H}^{-1}(\boldsymbol{\sigma}_e)\}\boldsymbol{\sigma}_e \tag{47}$$

Equation (45) is rewritten into

$$\begin{bmatrix} \dot{\boldsymbol{\omega}}_e \\ \dot{\boldsymbol{\zeta}} \end{bmatrix} = \begin{bmatrix} \boldsymbol{A}(\boldsymbol{\rho}) & \boldsymbol{0} \\ \frac{1}{4}\boldsymbol{I}_3 & \boldsymbol{0} \end{bmatrix} \begin{bmatrix} \boldsymbol{\omega}_e \\ \boldsymbol{\zeta} \end{bmatrix} + \begin{bmatrix} \bar{\boldsymbol{B}}_1 \\ \boldsymbol{0} \end{bmatrix} \tilde{\boldsymbol{u}}' + \begin{bmatrix} \boldsymbol{E} \\ \epsilon\boldsymbol{I}_3 \end{bmatrix} \boldsymbol{w} \tag{48}$$

or compactly as

$$\dot{\tilde{\boldsymbol{x}}} = \tilde{\boldsymbol{A}}_e(\boldsymbol{\rho})\tilde{\boldsymbol{x}} + \boldsymbol{B}_e\boldsymbol{u}' + \tilde{\boldsymbol{E}}_e\boldsymbol{w} \tag{49}$$

where $\tilde{\boldsymbol{x}} := [\boldsymbol{\omega}_e^T \quad \boldsymbol{\zeta}^T]^T$ and

$$\tilde{\boldsymbol{A}}_e(\boldsymbol{\rho}) := \begin{bmatrix} \boldsymbol{A}(\boldsymbol{\rho}) & \boldsymbol{0} \\ \frac{1}{4}\boldsymbol{I}_3 & \boldsymbol{0} \end{bmatrix}, \quad \boldsymbol{B}_e := \begin{bmatrix} \bar{\boldsymbol{B}}_1 \\ \boldsymbol{0} \end{bmatrix}, \quad \tilde{\boldsymbol{E}}_e = \begin{bmatrix} \boldsymbol{E} \\ \epsilon\boldsymbol{I}_3 \end{bmatrix} \tag{50}$$

with

$$\left\| \frac{\mathrm{d}}{\mathrm{d}t}\{\boldsymbol{H}^{-1}(\boldsymbol{\sigma}_e)\}\boldsymbol{\sigma}_e \right\| \le \epsilon\|\boldsymbol{w}\|, \qquad \epsilon > 0 \tag{51}$$

Note that a previous study [31] introduced a virtual state $\boldsymbol{\xi}$ with $\dot{\boldsymbol{\xi}} \simeq \boldsymbol{H}^{-1}(\boldsymbol{\sigma}_e)\dot{\boldsymbol{\sigma}}_e$ and replaced $\boldsymbol{H}^{-1}(\boldsymbol{\sigma}_e)\boldsymbol{\sigma}_e$ by $\boldsymbol{\xi}$. This transformation can be realized in the open-loop system because the part $\boldsymbol{\xi}$ is eliminated by the premultiplied matrix $\tilde{\boldsymbol{A}}_e(\boldsymbol{\rho})$ (note that two blocks of the right half of $\tilde{\boldsymbol{A}}_e(\boldsymbol{\rho})$ are zero entries). However, in the closed-loop system, this transformation includes an approximation. To avoid such an approximation in the closed-loop system, this paper introduced a virtual state $\boldsymbol{\zeta} := \boldsymbol{H}^{-1}(\boldsymbol{\sigma}_e)\boldsymbol{\sigma}_e$ and embed the transformation error $(\mathrm{d}/\mathrm{d}t)\{\boldsymbol{H}^{-1}(\boldsymbol{\sigma}_e)\}\boldsymbol{\sigma}_e$ into the disturbance as that upper bound $\epsilon\boldsymbol{I}_3$. This paper selects the positive scalar ϵ as the upper bound of $(\mathrm{d}/\mathrm{d}t)\{\boldsymbol{H}^{-1}(\boldsymbol{\sigma}_e)\}\boldsymbol{\sigma}_e$ by numerical simulation results.

The goal of the GS control for the simpler LPV model in Eq. (49):

$$\boldsymbol{u}' = -\tilde{\boldsymbol{K}}(\boldsymbol{\rho})\tilde{\boldsymbol{x}} \tag{52}$$

is to consider both overall stability and control performance at the same time as with Eq. (42).

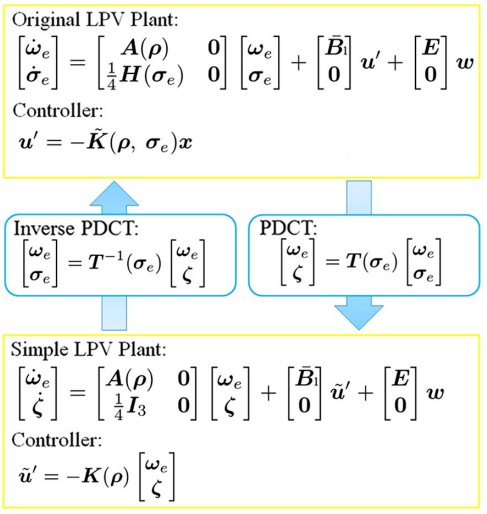

Fig. 3 Relationship between two models.

2. Relationship Between Original Model and Transformed Model

Getting back the coordinate transformation $\boldsymbol{x} := \boldsymbol{T}^{-1}(\boldsymbol{\sigma}_e)\tilde{\boldsymbol{x}}$, this GS controller can be transformed into the controller $\bar{\boldsymbol{K}}(\boldsymbol{\rho}, \boldsymbol{\sigma}_e)$ corresponding to the original plant in Eq. (35) as follows:

$$\boldsymbol{u}' = -\tilde{\boldsymbol{K}}(\boldsymbol{\rho})\boldsymbol{T}(\boldsymbol{\sigma}_e)\boldsymbol{T}^{-1}(\boldsymbol{\sigma}_e)\tilde{\boldsymbol{x}} \tag{53}$$

$$= -\bar{\boldsymbol{K}}(\boldsymbol{\rho}, \boldsymbol{\sigma}_e)\boldsymbol{x} \tag{54}$$

where

$$\bar{\boldsymbol{K}}(\boldsymbol{\rho}, \boldsymbol{\sigma}_e) := \tilde{\boldsymbol{K}}(\boldsymbol{\rho})\boldsymbol{T}(\boldsymbol{\sigma}_e) \tag{55}$$

This controller by method 2 is less approximated form and guarantees overall stability for closed system by introducing the transformation error as a disturbance. The relationship between original LPV plant as in Eq. (35) and transformed simple LPV plant as in Eq. (49) is shown as in Fig. 3. In this case, the number of scheduling parameters is reduced to 3 in Eq. (37), which yields $8(= 2^3)$ vertices and can design the optimal GS controller as with method 1.

3. Singularity Analysis of Transformation Matrix

The singularity of the PDCT matrix in Eq. (43) is analyzed. It is caused by the singularity of $\boldsymbol{H}^{-1}(\boldsymbol{\sigma}_e)$. From Eq. (23), $\boldsymbol{H}(\boldsymbol{\sigma}_e)$ has an inverse matrix except for the case of $\Phi = \pm 2\pi$. It can be easily avoided by introducing the shadow MRPs in analogy with the discussion of the Sec. II.B.

IV. Controller Synthesis

In the LPV control theory, first a convex hull constructed by the maximum and the minimum values of the scheduling parameters is introduced. Then, the extreme controllers defined at each vertex of the convex hull are designed by solving an LMI problem at each vertex. Finally, the optimal GS controller is constructed by the extreme controllers. To ensure overall stability for a whole operating range, a set of LMIs must be solved simultaneously. The number of LMIs of this set is equivalent to the number of vertices of the convex hull. There are generally too many vertices with the LPV model of a spacecraft attitude control problem. In the LPV model in Eq. (35), it has $64(= 2^6)$vertices. In this case, the LMIs become infeasible most possibly. On the other hand, the LMIs for the simple LPV models in Eqs. (40) and (49) are feasible most possibly. Let us consider the GS controller design for these simple LPV models.

A. Convex Hull

First, a convex hull constructed for the simple LPV model in Eq. (40) is considered. The scheduling parameter vector $\boldsymbol{\rho}$ of Eq. (37) has an interesting property. It can be represented by the spherical coordinate system as in Fig. 4. This property comes from DGVSCMG's spherical motion. Note that the wheel spin rate Ω represents the radial coordinate, and the inner/outer gimbal angles δ_i and δ_o represent the angular coordinate, which imply that the maximum and the minimum values of the scheduling parameters are determined as the limitation of the wheel spin rate, since the maximum values of the trigonometric functions of δ_i and δ_o are unity and the same is true with the minimum value. The LPV system in Eq. (40) and the GS controller in Eq. (42) are expressed by the following polytopic representation [23,26]:

$$\tilde{\boldsymbol{A}}_e(\boldsymbol{\rho}) = \sum_{i=1}^{p} \lambda_i(\boldsymbol{\rho})\tilde{\boldsymbol{A}}_{\mathrm{ei}} \tag{56}$$

$$\boldsymbol{K}(\boldsymbol{\rho}) = \sum_{i=1}^{p} \lambda_i(\boldsymbol{\rho})\boldsymbol{K}_i \tag{57}$$

$$\sum_{i=1}^{p} \lambda_i(\boldsymbol{\rho}) = 1, \qquad \lambda_i(\boldsymbol{\rho}) \geq 0 \tag{58}$$

where p denotes the number of vertices (in this case, p is equal to $8(= 2^3)$) and $\lambda_i(\boldsymbol{\rho})$ is the convex combination matrix given as in Table 1. Let $\underline{\rho}_i$ and $\bar{\rho}_i$ denote the lower and the upper bound of ρ_i. Using these parameters and introducing the following interpolation parameters $\underline{\alpha}_i$ and $\bar{\alpha}_i$, the scheduling parameters ρ_i can be described as follows:

$$\rho_i = \underline{\alpha}_i\underline{\rho}_i + \bar{\alpha}_i\bar{\rho}_i, \qquad 0 \leq \underline{\alpha}_i, \bar{\alpha}_i \leq 1, \qquad \underline{\alpha}_i + \bar{\alpha}_i = 1 \tag{59}$$

The extreme matrices $\tilde{\boldsymbol{A}}_{\mathrm{ei}}$, $1 \leq i \leq p$ in Eq. (56) are given by any frozen system of $\tilde{\boldsymbol{A}}(\boldsymbol{\rho})$ with any combination of $\bar{\rho}_i$ and $\underline{\rho}_i$ as in Table 1.

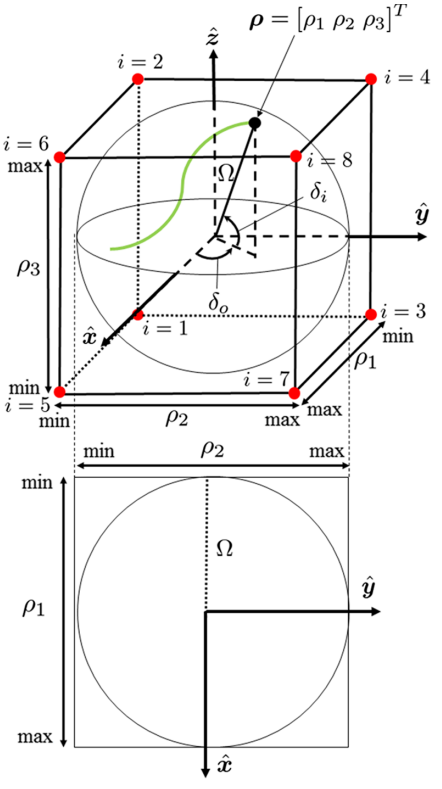

Fig. 4 Convex hull.

Table 1 Convex combination coefficients

i	$\boldsymbol{\rho}$	$\lambda_i(\boldsymbol{\rho})$	Binary
1	$[\underline{\rho}_1 \quad \underline{\rho}_2 \quad \underline{\rho}_3]^T$	$\underline{\alpha}_1\underline{\alpha}_2\underline{\alpha}_3$	000
2	$[\underline{\rho}_1 \quad \underline{\rho}_2 \quad \bar{\rho}_3]^T$	$\underline{\alpha}_1\underline{\alpha}_2\bar{\alpha}_3$	001
3	$[\underline{\rho}_1 \quad \bar{\rho}_2 \quad \underline{\rho}_3]^T$	$\underline{\alpha}_1\bar{\alpha}_2\underline{\alpha}_3$	010
4	$[\underline{\rho}_1 \quad \bar{\rho}_2 \quad \bar{\rho}_3]^T$	$\underline{\alpha}_1\bar{\alpha}_2\bar{\alpha}_3$	011
5	$[\bar{\rho}_1 \quad \underline{\rho}_2 \quad \underline{\rho}_3]^T$	$\bar{\alpha}_1\underline{\alpha}_2\underline{\alpha}_3$	100
6	$[\bar{\rho}_1 \quad \underline{\rho}_2 \quad \bar{\rho}_3]^T$	$\bar{\alpha}_1\underline{\alpha}_2\bar{\alpha}_3$	101
7	$[\bar{\rho}_1 \quad \bar{\rho}_2 \quad \underline{\rho}_3]^T$	$\bar{\alpha}_1\bar{\alpha}_2\underline{\alpha}_3$	110
8	$[\bar{\rho}_1 \quad \bar{\rho}_2 \quad \bar{\rho}_3]^T$	$\bar{\alpha}_1\bar{\alpha}_2\bar{\alpha}_3$	111

The extreme controllers $\boldsymbol{K}_{\text{ei}}$, $1 \le i \le p$ in Eq. (57) are designed for the extreme matrices $\tilde{\boldsymbol{A}}_{\text{ei}}$, $1 \le i \le p$ in Eq. (56), respectively. In this way, the convex hull that defines a whole operating range is constructed as shown in Fig. 4.

B. Extreme Controllers

A GS controller $\boldsymbol{K}(\boldsymbol{\rho})$ is desired that guarantees overall stability and achieves $\mathcal{H}_2$ performance for the simple LPV model in Eq. (40) with the performance output $\boldsymbol{z}$ as follows:

$$\dot{\boldsymbol{x}} = \tilde{\boldsymbol{A}}_e(\boldsymbol{\rho})\boldsymbol{x} + \boldsymbol{B}_e\boldsymbol{u}' + \boldsymbol{E}_e\boldsymbol{w} \tag{60a}$$

$$\boldsymbol{z} = \boldsymbol{C}\boldsymbol{x} + \boldsymbol{D}\boldsymbol{u}' \tag{60b}$$

The $\mathcal{H}_2$ control problem is considered. Let us consider the $\mathcal{H}_2$ norm as follows:

$$\|\boldsymbol{H}_{zw}(s)\|_2 = \int_0^\infty \boldsymbol{z}^T(t)\boldsymbol{z}(t)\,\mathrm{d}t \tag{61}$$

for an impulse disturbance input $\boldsymbol{w}$, and it is equivalent to

$$\|\boldsymbol{H}_{zw}(s)\|_2 = \int_0^\infty (\boldsymbol{x}^T\boldsymbol{C}^T\boldsymbol{C}\boldsymbol{x} + \boldsymbol{u}'^T\boldsymbol{D}^T\boldsymbol{D}\boldsymbol{u}')\,\mathrm{d}t \tag{62}$$

where the coefficient matrix set $(\boldsymbol{C}, \boldsymbol{D})$ is selected such that they satisfy the condition $\boldsymbol{C}^T\boldsymbol{D} = \boldsymbol{0}$, $\boldsymbol{D}^T\boldsymbol{D} > \boldsymbol{0}$. When the Lyapunov variable is time-varying and the optimal controller gain $\hat{\boldsymbol{K}}_i$ is introduced, minimizing $\|\boldsymbol{H}_{zw}(s)\|_2$ is equivalent to

$$\inf\left[\text{Trace}(\boldsymbol{B}_{\text{cl}}^T\boldsymbol{P}\boldsymbol{B}_{\text{cl}})\right] \quad \text{subject to} \tag{63}$$

$$\boldsymbol{P} > 0, \qquad \dot{\boldsymbol{P}} + \boldsymbol{P}\boldsymbol{A}_{\text{cl}} + \boldsymbol{A}_{\text{cl}}^T\boldsymbol{P} + \boldsymbol{C}_{\text{cl}}^T\boldsymbol{C}_{\text{cl}} < 0 \tag{64}$$

where

$$\boldsymbol{A}_{\text{cl}} = \tilde{\boldsymbol{A}}_{\text{ei}} - \boldsymbol{B}_e\boldsymbol{K}_i \tag{65}$$

$$\boldsymbol{B}_{\text{cl}} = \boldsymbol{E}_e \tag{66}$$

$$\boldsymbol{C}_{\text{cl}} = \boldsymbol{C} - \boldsymbol{D}\boldsymbol{K}_i \tag{67}$$

When the Lyapunov variable is time-invariant with $\dot{\boldsymbol{P}} = 0$, minimizing $\|\boldsymbol{H}_{zw}(s)\|_2$ is equivalent to

$$\inf\left[\text{Trace}(\boldsymbol{B}_{\text{cl}}^T\boldsymbol{P}\boldsymbol{B}_{\text{cl}})\right] \quad \text{subject to} \tag{68}$$

$$\boldsymbol{P} > 0, \qquad \boldsymbol{P}\boldsymbol{A}_{\text{cl}} + \boldsymbol{A}_{\text{cl}}^T\boldsymbol{P} + \boldsymbol{C}_{\text{cl}}^T\boldsymbol{C}_{\text{cl}} < 0 \tag{69}$$

For convenience, let us define the following matrix functions related to $\mathcal{H}_2$ performance. Pre- and postmultiply Eq. (69) by $\boldsymbol{X} = \boldsymbol{P}^{-1} > 0$; applying the Schur complement formula [32], Eq. (69) is equivalent to

$$\begin{bmatrix} (\tilde{\boldsymbol{A}}_{\text{ei}}\boldsymbol{X} - \boldsymbol{B}_e\boldsymbol{W}) + (\cdot)^T & * \\ \boldsymbol{C}\boldsymbol{X} - \boldsymbol{D}\boldsymbol{W} & -\boldsymbol{I} \end{bmatrix} < 0 \tag{70}$$

where $\boldsymbol{X}$ denotes the positive definite matrix and $\boldsymbol{W}$ denotes the rectangular matrix, $(\mathcal{A}) + (\mathcal{A})^T$ is abbreviated into $(\mathcal{A}) + (\cdot)^T$, and the symbol $*$ denotes the matrix symmetric element. Related to the $\mathcal{H}_2$ objective function in Eq. (68), introducing a slack variable $\boldsymbol{Z}$, Eq. (68) is equivalent to

$$\begin{bmatrix} \boldsymbol{X} & * \\ \boldsymbol{E}_e^T & \boldsymbol{Z} \end{bmatrix} > 0 \tag{71}$$

Here, to take into account the transient response of the control system, the LMI representation for the regional pole placement [33] is introduced as well as LMIs for $\mathcal{H}_2$ performance. The region [33] is the set $\boldsymbol{S}(\alpha, r, \Theta)$ of complex numbers $x + jy$ such that

$$x < -\alpha < 0, \qquad |x + jy| < r, \qquad \tan\Theta x < -|y| \tag{72}$$

as shown in Fig. 5. Confining the closed-loop poles to this region ensures the minimum decay rate α, the minimum damping ratio $\zeta = \cos\Theta$, a damped natural frequency $\omega_d < r\sin\theta$, and an undamped natural frequency $\omega_n < r$. This in turn bounds the maximum overshoot, the frequency of oscillatory modes, the delay time, the rise time, and the settling time. The LMIs for this regional pole placement are given by

$$(\tilde{\boldsymbol{A}}_{\text{ei}}\boldsymbol{X} - \boldsymbol{B}_e\boldsymbol{W}) + (\cdot)^T + 2\alpha\boldsymbol{X} < 0 \tag{73a}$$

$$\begin{bmatrix} -r\boldsymbol{X} & \tilde{\boldsymbol{A}}_{\text{ei}}\boldsymbol{X} - \boldsymbol{B}_e\boldsymbol{W} \\ * & -r\boldsymbol{X} \end{bmatrix} < 0 \tag{73b}$$

$$\begin{bmatrix} \boldsymbol{\Gamma}(\Theta) & \tilde{\boldsymbol{\Gamma}}(\Theta) \\ * & \boldsymbol{\Gamma}(\Theta) \end{bmatrix} < 0 \tag{73c}$$

where

$$\boldsymbol{\Gamma}(\Theta) = \sin\Theta\left\{(\tilde{\boldsymbol{A}}_{\text{ei}}\boldsymbol{X} - \boldsymbol{B}_e\boldsymbol{W}) + (\cdot)^T\right\} \tag{74}$$

$$\tilde{\boldsymbol{\Gamma}}(\Theta) = \cos\Theta\left\{(\tilde{\boldsymbol{A}}_{\text{ei}}\boldsymbol{X} - \boldsymbol{B}_e\boldsymbol{W}) - (\cdot)^T\right\} \tag{75}$$

which enable us to easily specify the closed-loop time response with the stability margin α.

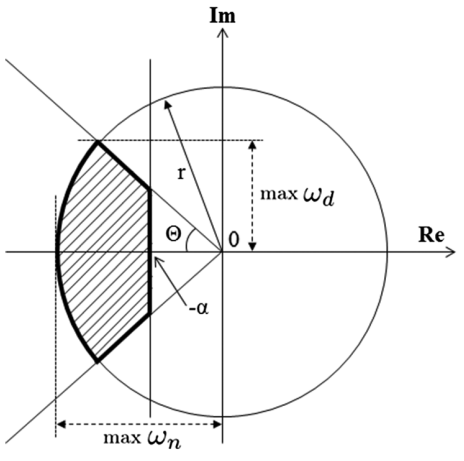

Fig. 5 Regional pole placement.

In this study, the LMI problem represented by both $\mathcal{H}_2$ control in Eqs. (70) and (71) and the regional pole placement in Eq. (73) is considered as follows:

$$\inf_{\boldsymbol{W}_i,\boldsymbol{X},\boldsymbol{Z}}[\mathrm{Trace}(\boldsymbol{Z})] \quad \text{subject to} \tag{76a}$$

$$\begin{bmatrix} (\tilde{\boldsymbol{A}}_{\mathrm{ei}}\boldsymbol{X}-\boldsymbol{B}_e\boldsymbol{W}_i)+(\cdot)^T & * \\ \boldsymbol{C}\boldsymbol{X}-\boldsymbol{D}\boldsymbol{W}_i & -\boldsymbol{I} \end{bmatrix}<0, \quad \begin{bmatrix} \boldsymbol{X} & * \\ \boldsymbol{E}_e^T & \boldsymbol{Z} \end{bmatrix}>0 \tag{76b}$$

$$(\tilde{\boldsymbol{A}}_{\mathrm{ei}}\boldsymbol{X}-\boldsymbol{B}_e\boldsymbol{W}_i)+(\cdot)^T+2\alpha\boldsymbol{X}<0 \tag{76c}$$

$$\begin{bmatrix} -r\boldsymbol{X} & \tilde{\boldsymbol{A}}_{\mathrm{ei}}\boldsymbol{X}-\boldsymbol{B}_e\boldsymbol{W}_i \\ * & -r\boldsymbol{X} \end{bmatrix}<0, \quad \begin{bmatrix} \boldsymbol{\Gamma}_i(\Theta) & \tilde{\boldsymbol{\Gamma}}_i(\Theta) \\ * & \boldsymbol{\Gamma}_i(\Theta) \end{bmatrix}<0, \quad \text{for all } 1\le i\le 8 \tag{76d}$$

where

$$\boldsymbol{\Gamma}_i(\Theta)=\sin\Theta\left\{(\tilde{\boldsymbol{A}}_{\mathrm{ei}}\boldsymbol{X}-\boldsymbol{B}_e\boldsymbol{W}_i)+(\cdot)^T\right\} \tag{77}$$

$$\tilde{\boldsymbol{\Gamma}}_i(\Theta)=\cos\Theta\left\{(\tilde{\boldsymbol{A}}_{\mathrm{ei}}\boldsymbol{X}-\boldsymbol{B}_e\boldsymbol{W}_i)-(\cdot)^T\right\} \tag{78}$$

Using the optimal solution set $\boldsymbol{X}, \boldsymbol{W}_i$ to the problem in Eq. (76), the extreme controller of the convex hull are given by

$$\boldsymbol{K}_i=\boldsymbol{W}_i\boldsymbol{X}^{-1}, \qquad 1\le i\le 8 \tag{79}$$

Then, the GS controller with method 1 in Eq. (42) is constructed by substituting Eq. (79) into Eq. (57). Therefore, the optimal GS controller for the simple LPV model in Eq. (40) is obtained by

$$\boldsymbol{u}'=-\boldsymbol{K}(\boldsymbol{\rho})\boldsymbol{x} \tag{80}$$

Similarly, the GS controller with method 2 in Eq. (52) can be obtained as follows:

$$\boldsymbol{u}'=-\tilde{\boldsymbol{K}}(\boldsymbol{\rho})\tilde{\boldsymbol{x}}, \qquad \tilde{\boldsymbol{x}}=\boldsymbol{T}(\boldsymbol{\sigma}_e)\boldsymbol{x} \tag{81}$$

for the simple LPV model in Eq. (49).

V. Steering Law Design

First, this section provides the singularity of a DGVSCMG, and then a singularity avoidance steering law of a DGVSCMG and MTQs is proposed.

A. Singularity Analysis of a DGVSCMG

The singularity of a DGVSCMG is considered. From Eq. (31), the Jacobian matrix of the DGVSCMG system is given by

$$\boldsymbol{N}_1=\begin{bmatrix} \cos\delta_i\cos\delta_o & -\Omega\sin\delta_i\cos\delta_o & -\Omega\cos\delta_i\sin\delta_o \\ \cos\delta_i\sin\delta_o & -\Omega\sin\delta_i\sin\delta_o & \Omega\cos\delta_i\cos\delta_o \\ -\sin\delta_i & -\Omega\cos\delta_i & 0 \end{bmatrix} \tag{82}$$

Previously, the steering law of a single DGVSCMG system is given by

$$\boldsymbol{u}_{\mathrm{DGV}}=N_1^{-1}\boldsymbol{u}' \tag{83}$$

If rank $(\boldsymbol{N}_1)=3$, the inverse matrix $\boldsymbol{N}_1^{-1}$ can be always obtained. However, if the rank $(\boldsymbol{N}_1)\neq 3$ then this cannot be solved. It occurs when $\det(\boldsymbol{N}_1)=0$ with

$$\det(\boldsymbol{N}_1)=-\Omega^2\cos\delta_i \tag{84}$$

When the spin rate is zero ($\Omega=0$) or the inner and outer gimbals are overlapped ($\cos\delta_i=0$), the DGVSCMG system falls into a singularity.

B. Singularity Avoidance Steering Law

Recalling in Eq. (33), the output torque is given by

$$\boldsymbol{u}'=\boldsymbol{N}_1\boldsymbol{u}_{\mathrm{DGV}}+\bar{\boldsymbol{B}}_1^{-1}\bar{\boldsymbol{B}}_2\boldsymbol{N}_2\boldsymbol{m}_{\mathrm{MTQ}} \tag{85}$$

By using the inverse matrix of $\boldsymbol{N}_1$, the DGVSCMG input is given by

$$\boldsymbol{u}_{\mathrm{DGV}}=\boldsymbol{N}_1^{-1}\boldsymbol{u}'-\boldsymbol{N}_1^{-1}\bar{\boldsymbol{B}}_1^{-1}\bar{\boldsymbol{B}}_2\boldsymbol{N}_2\boldsymbol{m}_{\mathrm{MTQ}} \tag{86}$$

where this is the steering law of the DGVSCMG. When $\det(\boldsymbol{N}_1)=0$, the steering law in Eq. (86) cannot be solved. To avoid such a situation, the singularity robustness (SR) steering law [3] is considered as follows:

$$\boldsymbol{u}_{\mathrm{DGV}}=\boldsymbol{N}_1^{\#}\boldsymbol{u}'-\boldsymbol{N}_1^{\#}\bar{\boldsymbol{B}}_1^{-1}\bar{\boldsymbol{B}}_2\boldsymbol{N}_2\boldsymbol{m}_{\mathrm{MTQ}} \tag{87}$$

where

$$\boldsymbol{N}_1^{\#}=\boldsymbol{N}_1^T(\boldsymbol{N}_1\boldsymbol{N}_1^T+\lambda_1\boldsymbol{I})^{-1} \tag{88}$$

$$\lambda_1=k_1\exp(-k_1'|\det(\boldsymbol{N}_1)|) \tag{89}$$

where k_1 and k_1' are positive scalars. When $|\det(\boldsymbol{N}_1)|$ is larger enough, Eq. (87) is approaching to Eq. (86). Although this SR steering law is intended to avoid the singularity by adding torque errors, it is not guaranteed to steer gimbal angles or manage the wheel spin rate from their singularities. To manage the gimbal angles and the wheel spin rate, the following Lyapunov function $V(>0)$ is considered:

$$V=\frac{1}{2}\boldsymbol{u}_e^T\boldsymbol{u}_e \tag{90}$$

with

$$\boldsymbol{u}_e=\begin{bmatrix} \Omega-\Omega_r \\ \delta_i-\delta_{ir} \\ 0 \end{bmatrix} \tag{91}$$

where Ω_r and δ_{ir} are the preferred wheel spin rate and inner gimbal angle, respectively. The time derivative of Eq. (90) is given by

$$\dot{V}=\boldsymbol{u}_e^T\boldsymbol{u}_{\mathrm{DGV}} \tag{92}$$

since the preferred set Ω_r, δ_{ir} is constant. To guarantee Lyapunov stability $\dot{V}<0$ for attaining the preferred set, the DGVSCMG actuator input for avoiding the singularity is given by

$$\boldsymbol{u}_{\mathrm{DGV}}=-\bar{\boldsymbol{W}}\boldsymbol{u}_e \tag{93}$$

with

$$\bar{\boldsymbol{W}}=\begin{bmatrix} b_1 & 0 & 0 \\ 0 & b_2 & 0 \\ 0 & 0 & 0 \end{bmatrix} \tag{94}$$

where $\bar{\boldsymbol{W}}$ is the weighting matrix with the positive scalars b_1 and b_2. In this case, the time derivative of the Lyapunov function V is given by

$$\dot{V}=-\boldsymbol{u}_e^T\bar{\boldsymbol{W}}\boldsymbol{u}_e\le 0 \tag{95}$$

Combining Eqs. (83) and (93) while introducing an SR steering method, the steering law of a DGVSCMG for avoiding the singularity is given by

$$\boldsymbol{u}_{\mathrm{DGV}}=\boldsymbol{N}_1^{\#}\boldsymbol{u}'-\bar{\boldsymbol{W}}\boldsymbol{u}_e \tag{96}$$

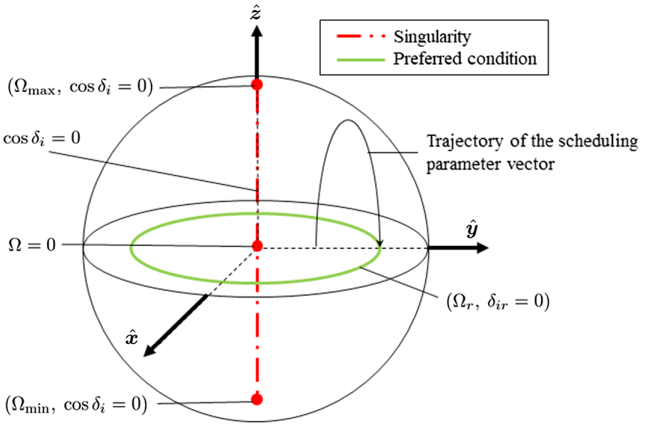

Fig. 6 Illustration of the scheduling parameter vector.

In general, a steering law tends to use the null space (for instance, with the local gradient method) if it is available, not to prevent the three-axis attitude control [3]. However, the steering law is certainly not robust with only single DGVSCMG as there is no null space to avoid the singularity. Previous research [13,14] discussed this singularity avoidance as a future work. This study attempts to avoid the singularity by using MTQ torques. From Eqs. (87) and (93), the steering law for avoiding the singularity is obtained by

$$\boldsymbol{u}_{\mathrm{DGV}} = \boldsymbol{N}_1^{\#}\boldsymbol{u}' - \bar{\boldsymbol{W}}\boldsymbol{u}_e - \boldsymbol{N}_1^{\#}\bar{\boldsymbol{B}}_1^{-1}\bar{\boldsymbol{B}}_2\boldsymbol{N}_2\boldsymbol{m}_{\mathrm{MTQ}} \tag{97}$$

The MTQ input to eliminate the term $-\bar{\boldsymbol{W}}\boldsymbol{u}_e$ is given by

$$-\bar{\boldsymbol{W}}\boldsymbol{u}_e - \boldsymbol{N}_1^{\#}\bar{\boldsymbol{B}}_1^{-1}\bar{\boldsymbol{B}}_2\boldsymbol{N}_2\boldsymbol{m}_{\mathrm{MTQ}} = 0 \tag{98}$$

$$\boldsymbol{m}_{\mathrm{MTQ}} = -\boldsymbol{N}_2^{\#}\bar{\boldsymbol{B}}_2^{-1}\bar{\boldsymbol{B}}_1\boldsymbol{N}_1\bar{\boldsymbol{W}}\boldsymbol{u}_e \tag{99}$$

where

$$\boldsymbol{N}_2^{\#} = \boldsymbol{N}_2^T(\boldsymbol{N}_2\boldsymbol{N}_2^T + k_2\boldsymbol{I})^{-1}, \qquad k_2 > 0 \tag{100}$$

Note that an MTQ steering always falls in the singularity, so again the SR steering inverse is adapted. Figure 6 shows the illustration of the scheduling parameter vector in Eq. (37). The proposed steering laws in Eqs. (97) and (99) give the trajectory to the preferred condition that is away from the singularities.

VI. Numerical Simulation

This section presents some numerical simulations by using the GS controllers with method 1 in Eq. (80) and method 2 in Eq. (81) and also compares the conventional steering law in Eq. (83), the SR steering law in Eq. (96), and the SR steering law with MTQs in Eqs. (97) and (99).

A. Simulation Parameters

The controller design parameters $\boldsymbol{C}$ and $\boldsymbol{D}$, and the disturbance coefficient matrices $\boldsymbol{E}_e$ and $\tilde{\boldsymbol{E}}_e$ are given as follows:

$$\boldsymbol{C} = \begin{bmatrix} 3\times\boldsymbol{I}_3 & 0_{3\times3} \\ 0_{3\times3} & \boldsymbol{I}_3 \\ 0_{3\times3} & 0_{3\times3} \end{bmatrix}, \quad \boldsymbol{D} = \begin{bmatrix} 0_{6\times3} \\ 0.02\times\boldsymbol{I}_3 \end{bmatrix},$$
$$\boldsymbol{E}_e = \begin{bmatrix} \mathrm{diag}[2.15.51.7]\times10^{-5} \\ 0_{3\times3} \end{bmatrix}, \quad \tilde{\boldsymbol{E}}_e = \begin{bmatrix} \mathrm{diag}[2.15.51.7]\times10^{-5} \\ \boldsymbol{I}_3 \end{bmatrix} \tag{101}$$

Note that the disturbance coefficient matrices $\boldsymbol{E}_e$ and $\tilde{\boldsymbol{E}}_e$ are determined by the maximum value of the following environmental torque disturbance vector [20]:

$$\boldsymbol{\tau}_d = \begin{bmatrix} 12.8\times10^{-6} + 8.6\times10^{-6}\sin nt \\ 5.5\times10^{-5}(1+\sin nt) \\ 12.8\times10^{-6} + 4.3\times10^{-6}\sin nt \end{bmatrix} \mathrm{N\cdot m} \tag{102}$$

and ϵ in $\tilde{\boldsymbol{E}}_e$ is determined as $\epsilon = 1$, which is an enough large value by simulation results. The parameters of the regional pole placement in Eqs. (76c) and (76d) are given by

$$r = 1.0, \quad \alpha = 0.1, \quad \Theta = \frac{\pi}{4} \tag{103}$$

and the parameters of the proposed singularity avoidance steering laws in Eqs. (97) and (99) are given by

$$k_1 = 10, \quad k_1' = 0.001, \quad k_2 = 0.01, \quad b_1 = 1, \quad b_2 = 0.1 \tag{104}$$

with the preferred wheel spin rate and the inner gimbal angle:

$$\Omega_r = 300\ \mathrm{rpm}, \quad \delta_{ir} = 0\ \mathrm{rad} \tag{105}$$

The simulation parameters are given in Table 2, in which the initial condition of the error angular velocity of the spacecraft and actuator conditions are also given. The orbital parameters are given in Table 3, in which these parameters closely parallel those used in Ref. [20] and the total dipole strength is also given. The limitation of DGVSCMG and MTQ input is given by

$$-10 \le \dot{\Omega} \le 10\ \mathrm{rad/s^2}, \quad -1 \le \dot{\delta}_i \le 1\ \mathrm{rad/s}, \quad -1 \le \dot{\delta}_o \le 1\ \mathrm{rad/s} \tag{106a}$$

$$-10^{-3} \le m_{\mathrm{MTQ},i} \le 10^{-3}\ \mathrm{A\cdot m^2}, \quad 1 \le i \le 3 \tag{106b}$$

This simulation also considers the model uncertainty $\Delta[J]$ on the inertia tensor $[J]$. Therefore, in the numerical simulation, the inertia tensor $[J]$ is given by $[J] + \Delta[J]$ with $\Delta[J] = 0.2[J]$, because the moments and products of inertia of the spacecraft may change due to fuel usage or solar paddle oscillations.

Table 2 Simulation parameters

Parameter	Value	Unit
$^{\mathcal{B}}[I_s]$	diag[10 10 8]	kg · m^2
$^{\mathcal{G}_i}[I_{\mathrm{ws}}]$	diag[0.0042 0.0021 0.0021]	kg · m^2
$^{\mathcal{G}_i}[I_{\mathrm{gi}}]$	diag[0.001 0.001 0.001]	kg · m^2
$^{\mathcal{G}_o}[I_{\mathrm{go}}]$	diag[0.001 0.001 0.001]	kg · m^2
Ω_0	250	rad/s
δ_{i0}	0	rad
δ_{o0}	0	rad
$\boldsymbol{\omega}_{e0}$	$[0\ \ 0\ \ 0]^T$	rad/s

Table 3 Orbital parameters

Parameter	Value	Unit
μ	7.9×10^{15}	Wb · m
a	7359.42	km
i	53	deg
n	0.001	rad/s

B. Three-Axis Attitude Control Simulation

Figure 7 shows the attitude maneuver simulation results with the initial error MRPs $\boldsymbol{\sigma}_{e0} = [0.414 \quad 0.3 \quad 0.2]^T$ in Ref. [10] by using the GS controller in Eq. (81) and the singularity avoidance steering laws in Eqs. (97) and (99). From the time history of the angular velocity in (a) and the error MRPs in (b), the three-axis attitude control has been successfully achieved at 40 s. Subfigures (c) and (d) in Fig. 7 represent the gimbal angles and rates (gimbal input), respectively. Subfigures (e) and (f) in Fig. 7 represent the wheel spin rate and acceleration (wheel input), respectively. From subfigures (c) and (e) in Fig. 7, the preferred set of a DGVSCMG in Eq. (105) is obtained by the proposed steering laws while avoiding the singularities in (h) in Fig. 7. Besides, the limitation of the actuator input in Eq. (106) has not exceeded in (d), (f), and (g) in Fig. 7.

C. Comparison of Steering Laws

Figure 8 shows the attitude maneuver simulation results with the initial error MRPs $\boldsymbol{\sigma}_{e0} = [0.252 \quad 0 \quad -0.092]^T$ as one of the initial conditions that shall fall into the singularity. This subsection presents three types of simulation results by using the conventional steering law in Eq. (83), the SR steering law in Eq. (96), and the SR steering law with MTQs in Eqs. (97) and (99). The singularity measurement $\det(\boldsymbol{N}_1)$ is shown as in subfigure (a) in Fig. 8. When $\det(\boldsymbol{N}_1) = 0$, the system falls into the singularity. MRPs are shown as in subfigure (b) in Fig. 8 and the inner/outer gimbal angles and wheel spin rate are shown as in subfigures (c), (d), and (e) in Fig. 8, respectively. From Fig. 8, the conventional steering law in Eq. (83) falls into singularity at 25 s and cannot attain three-axis attitude control, because the wheel spin rate is approaching to zero at that time. The SR steering law in Eq. (96) can successfully avoid the singularity but cannot attain three-axis attitude control, because it has no null space and the steering motion for avoiding the singularity prevents the spacecraft from achieving the attitude control. On the other hand, the SR steering law with MTQs in Eqs. (97) and (99) successfully achieves both singularity avoidance and complete attitude control, because the proposed steering law provides preferred set of a DGVSCMG ($\Omega = 300$ rpm and $\delta_i = 0$ rad). Therefore, the effectiveness of the proposed steering law in Eqs. (97) and (99) is shown as in Fig. 8.

D. Monte Carlo Simulation

Figure 9 shows the 614-run Monte Carlo (MC) simulation result given by a variety of rotation angles generated by a variety of combinations of initial and final attitudes of the spacecraft. This MC

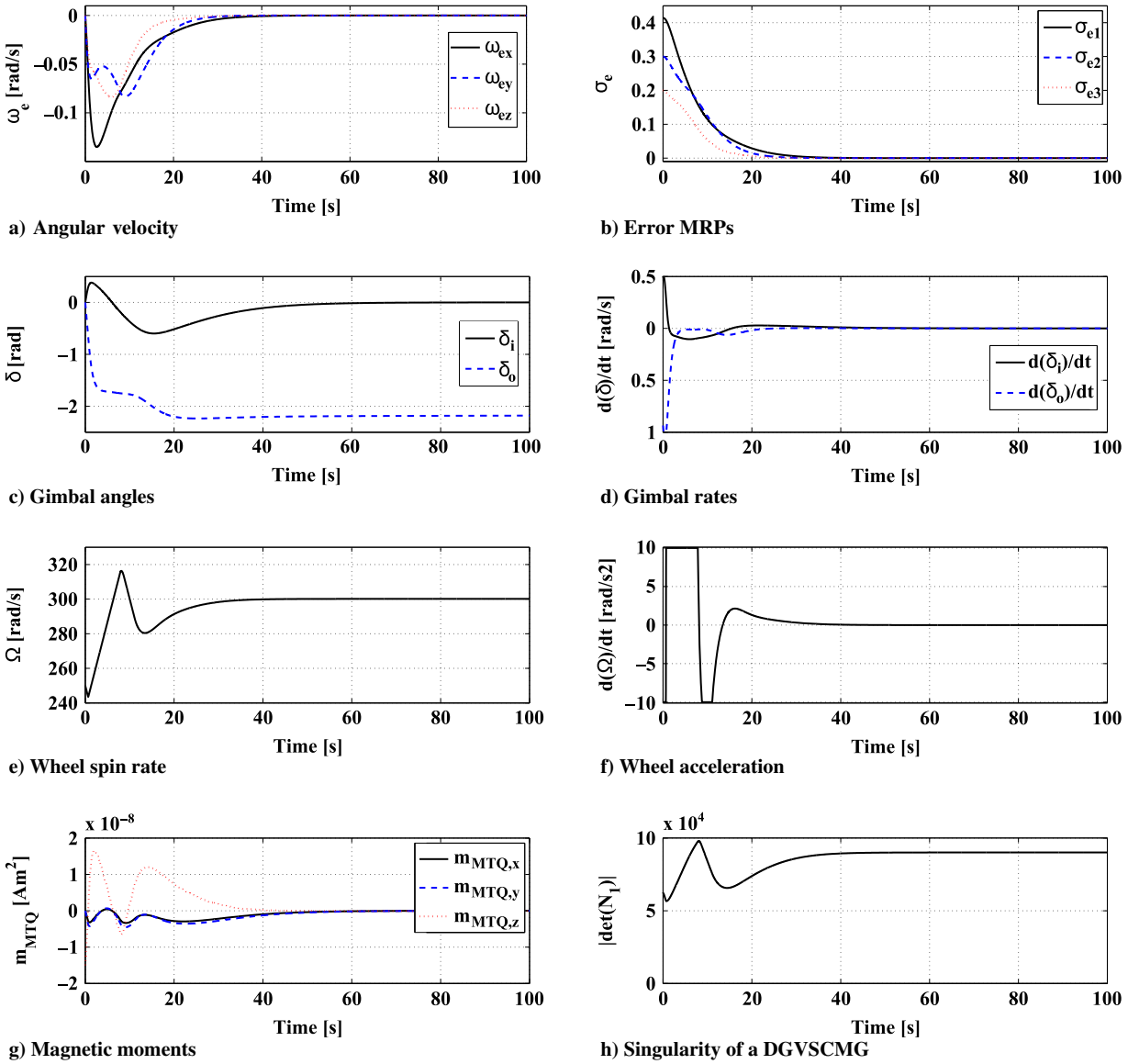

Fig. 7 Attitude simulation.

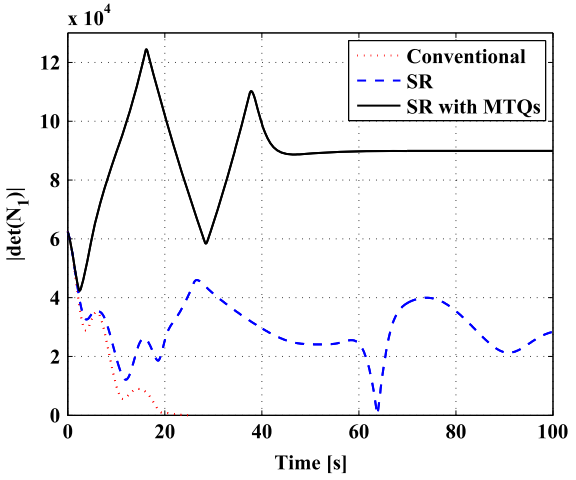

a) Singularity measurement

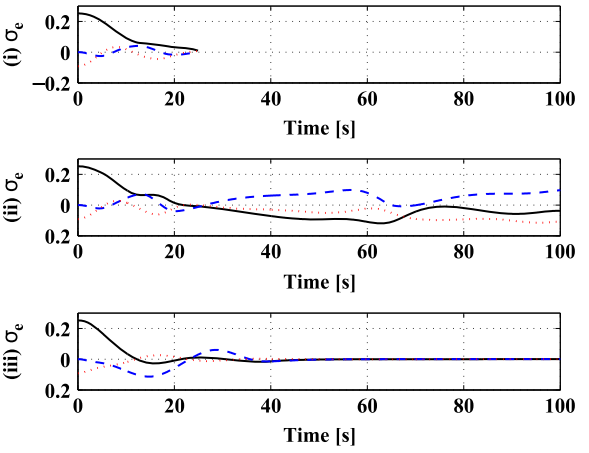

b) MRPs by using (i) conventional steering law, (ii) SR steering law, and (iii) SR steering law with MTQs

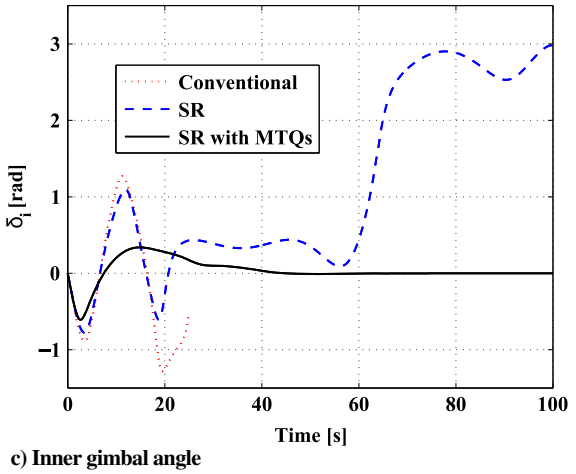

c) Inner gimbal angle

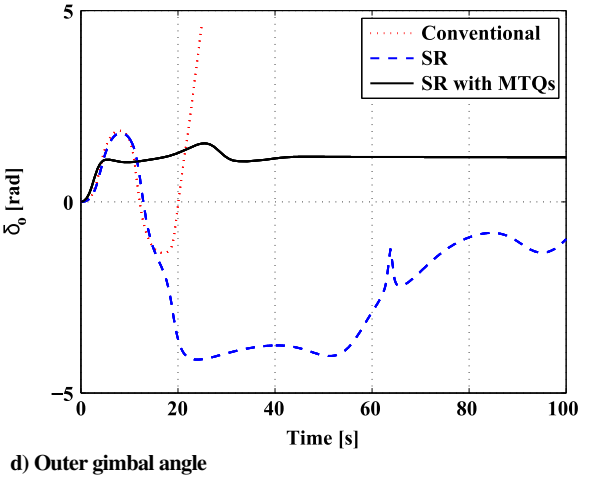

d) Outer gimbal angle

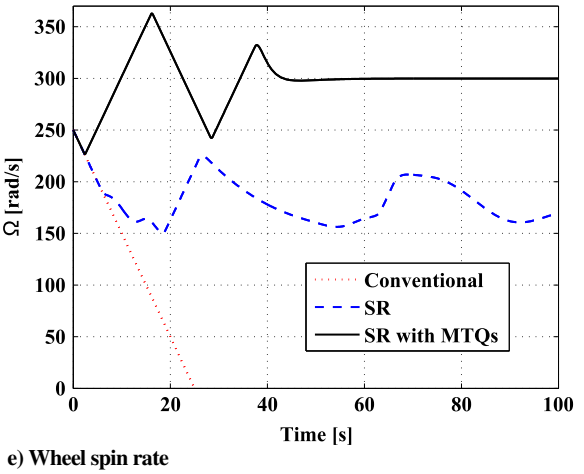

e) Wheel spin rate

Fig. 8 Comparison of the steering laws.

simulation aims to compare the two proposed methods by using the GS controllers in Eqs. (80) and (81). This figure shows the rotation angle φ versus the average of the convergence time t^*. From this figure in the small attitude maneuver ($\varphi \leq 90$ deg), these controllers attain three-axis attitude control at almost the same time because the GS controller of method 2 in Eq. (81) can be approximated by that of method 1 in Eq. (80) by using the following approximation of the PDCT matrix:

$$\boldsymbol{T}(\boldsymbol{\sigma}_e) \simeq \boldsymbol{I}_6 \tag{107}$$

On the other hand, in the large attitude maneuver, the convergence time of method 2 with PDCT is shorter than that of method 1, because method 1 includes approximation in the modeling of the LPV plant. This approximation is useful for the small attitude maneuver but not good for the large attitude maneuver when the model error becomes

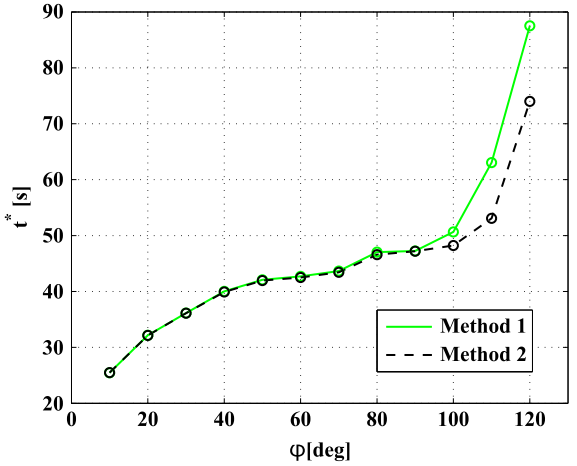

Fig. 9 Comparison of the convergence time.

large. Therefore, method 2 with PDCT can attain preferred control performance for all three-axis attitude rotations, compared with method 1. On the other hand, in the case of the small attitude maneuver such as an attitude tracking problem, method 1 is also good as an easy-to-use controller design.

VII. Conclusions

This paper derives a linear parameter-varying (LPV) model for three-axis attitude control of a spacecraft with a double-gimbal variable-speed control moment gyroscope (DGVSCMG) and magnetic torquers (MTQs). Based on this LPV model, two types of simple LPV models are established to design gain-scheduled controllers by using two methods. These two methods overcome the difficulty from excess of the number of scheduling parameters. Besides, the singularity avoidance steering laws of a DGVSCMG by using MTQs is proposed. Through the Monte Carlo simulation examples, the effectiveness of the LPV model with the parameter-dependent coordinate transformation and the singularity avoidance steering law are demonstrated. Future work will consider translational motion of the center of mass of the flexible structures and a gain tuning method for the GS controller and the singularity avoidance steering law.

Acknowledgment

This work was supported by JSPS Grant-in-Aid for Scientific Research Grant Numbers 15J11371 and (C)15K06149.

References

[1] Schaub, H., and Lappas, J. V., "Redundant Reaction Wheel Torque Distribution Yielding Instantaneous L_2 Power-Optimal Attitude Control," *Journal of Guidance, Control, and Dynamics*, Vol. 32, No. 4, July–Aug. 2009, pp. 1269–1276. doi:10.2514/1.41070

[2] Blenden, R., and Schaub, H., "Regenerative Power-Optimal Reaction Wheel Attitude Control," *Journal of Guidance, Control, and Dynamics*, Vol. 35, No. 4, July–Aug. 2012, pp. 1208–1217. doi:10.2514/1.55493

[3] Wie, B., Bailey, D., and Heiberg, C., "Singularity Robust Steering Logic for Redundant Single-Gimbal Control Moment Gyros," *Journal of Guidance, Control, and Dynamics*, Vol. 24, No. 5, Sept.–Oct. 2001, pp. 865–872. doi:10.2514/2.4799

[4] Kurokawa, H., "Survey of Theory and Steering Laws of Single-Gimbal Control Moment Gyros," *Journal of Guidance, Control, and Dynamics*, Vol. 30, No. 5, Sept.–Oct. 2007, pp. 1331–1340. doi:10.2514/1.27316

[5] Ford, K. A., and Hall, C. D., "Singular Direction Avoidance Steering for Control Moment Gyros," *Journal of Guidance, Control, and Dynamics*, Vol. 23, No. 4, 2000, pp. 648–656. doi:10.2514/2.4610

[6] Okubo, H., and Tani, Y., "Singularity Robust Steering of Redundant Single Gimbal Control Moment Gyros for Small Satellites," *Proceedings of the 8th International Symposium on Artificial Intelligence, Robotics and Automation in Space* [CDROM], edited by B. Battrick, European Space Agency ESA SP-603, Munich, 2005.

[7] Marshall, A., and Tsiotras, P., "Spacecraft Angular Velocity Stabilization Using a Single-Gimbal Variable Speed Control Moment Gyro," *AIAA Guidance, Navigation, and Control Conference and Exhibit*, AIAA Paper 2003-5654, 2003.

[8] Yamada, K., Takatsuka, N., and Shima, T., "Spacecraft Pointing Control Using a Variable-Speed Control Moment Gyro," *Transactions of Space Technology Japan*, Vol. 7, No. ists26, 2009, pp. Pd_1–Pd_6.

[9] Yoon, H., and Tsiotras, P., "Singularity Analysis of Variable-Speed Control Moment Gyros," *Journal of Guidance, Control, and Dynamics*, Vol. 27, No. 3, May–June 2004, pp. 374–386. doi:10.2514/1.2946

[10] Schaub, H., Vadali, R. S., and Junkins, L. J., "Feedback Control Law for Variable Speed Control Moment Gyros," *Journal of the Astronautical Sciences*, Vol. 46, No. 3, July–Sept. 1998, pp. 307–328.

[11] Schaub, H., and Junkins, L. J., "Singularity Avoidance Using Null Motion and Variable-Speed Control Moment Gyros," *Journal of Guidance, Control, and Dynamics*, Vol. 23, No. 1, Jan.–Feb. 2000, pp. 11–16. doi:10.2514/2.4514

[12] Ahmed, J., and Bernstein, D., "Adaptive Control of Double-Gimbal Control-Moment Gyro with Unbalanced Rotor," *Journal of Guidance, Control, and Dynamics*, Vol. 25, No. 1, Jan.–Feb. 2002, pp. 105–115. doi:10.2514/2.4855

[13] Stevenson, D., and Schaub, H., "Nonlinear Control Analysis of a Double-Gimbal Variable-Speed Control Moment Gyroscope," *Journal of Guidance, Control, and Dynamics*, Vol. 35, No. 3, May–June 2012, pp. 787–793. doi:10.2514/1.56104

[14] Zhang, H., and Fang, J., "Robust Backstepping Control for Agile Satellite Using Double-Gimbal Variable-Speed Control Moment Gyroscope," *Journal of Guidance, Control, and Dynamics*, Vol. 36, No. 5, Sept.–Oct. 2013, pp. 1356–1363. doi:10.2514/1.59327

[15] Jikuya, I., Fujii, K., and Yamada, K., "Attitude Maneuver of Spacecraft with a Variable-Speed Double-Gimbal Ccontrol Mmoment Gyro," *Advances in Space Research*, Vol. 58, No. 7, Oct. 2016, pp. 1303–1317. doi:10.1016/j.asr.2016.06.010

[16] Sasaki, T., and Shimomura, T., "Attitude Control of a Spacecraft with a Double-Gimbal Variable-Speed Control Moment Gyro via LPV Control Theory," *Advances in the Astronautical Sciences*, Vol. 153, 2015, pp. 707–723.

[17] Cui, P., and He, J., "Steering Law for Two Parallel Variable-Speed Double-Gimbal Control Moment Gyros," *Journal of Guidance, Control, and Dynamics*, Vol. 37, No. 1, Jan.–Feb. 2014, pp. 350–359. doi:10.2514/1.60403

[18] Sasaki, T., and Shimomura, T., "Fault-Tolerant Architecture of Two Parallel Double-Gimbal Variable-Speed Control Moment Gyros," *AIAA Guidance, Navigation, and Control Conference, AIAA SciTech Forum*, AIAA Paper 2016-0090, 2016. doi:10.2514/6.2016-0090

[19] Celani, F., "Robust Three-Axis Attitude Stabilization for Inertial Pointing Spacecraft Using Magnetorquers," *Acta Astronautica*, Vol. 107, Feb.–March 2015, pp. 87–96. doi:10.1016/j.actaastro.2014.11.027

[20] Tewari, A., and Renuganth, V., "Optimal Attitude Control Through Magnetic Torquers and Reaction Wheels," *IFAC Proceedings Volumes*, Vol. 40, No. 7, 2007, pp. 19–24. doi:10.3182/20070625-5-FR-2916.00005

[21] Tsiotras, P., "Stabilization and Optimality Results for the Attitude Control Problem," *Journal of Guidance, Control, and Dynamics*, Vol. 19, No. 4, July–Aug. 1996, pp. 772–779. doi:10.2514/3.21698

[22] Yoon, H., and Tsiotras, P., "Spacecraft Line-of-Sight Control Using a Single Variable-Speed Control Moment Gyro," *Journal of Guidance, Control, and Dynamics*, Vol. 29, No. 6, Nov.–Dec. 2006, pp. 1295–1308. doi:10.2514/1.18777

[23] Apkarian, P., Gahinet, P., and Becker, G., "Self-Scheduled $\mathcal{H}_\infty$ Control of Linear Parameter-Varying Systems: A Design Example," *Automatica*, Vol. 31, No. 9, Sept. 1995, pp. 1251–1261. doi:10.1016/0005-1098(95)00038-X

[24] Shimomura, T., and Kubotani, T., "Gain-Scheduled Control under Common Lyapunov Functions: Conservatism Revisited," *Proceedings of 2005 American Control Conference*, IEEE Paper WeB10.4, Portland, OR, 2005, pp. 870–875. doi:10.1109/ACC.2005.1470069

[25] Sasaki, T., Schaub, H., and Shimomura, T., "Convex Optimization of a Spacecraft Stabilization with a Double-Gimbal Variable-Speed Control

Moment Gyro Actuator: Geometric Approach," *IEEE Conference on Control Technology and Applications*, IEEE Paper TB1.6, Kohala Coast, HI, 2017.

[26] Kwon, S., Shimomura, T., and Okubo, H., "Pointing Control of Spacecraft Using Two SGCMGs via LPV Control Theory," *Acta Astronautica*, Vol. 68, Nos. 7–8, 2011, pp. 1168–1175. doi:10.1016/j.actaastro.2010.10.001

[27] Navabi, M., and Barati, M., "Mathematical Modeling and Simulation of the Earth's Magnetic Field: A Comparative Study of the Models on the Spacecraft Attitude Control Application," *Applied Mathematical Modelling*, Vol. 46, June 2017, pp. 365–381. doi:10.1016/j.apm.2017.01.040

[28] Schaub, H., and Junkins, J. L., *Analytical Mechanics of Space Systems*, 3rd ed., AIAA Education Series, AIAA, Reston, VA, 2014, pp. 117–126. doi:10.2514/4.102400

[29] Schaub, H., and Junkins, J. L., "Stereographic Orientation Parameters for Attitude Dynamics: A Generalization of the Rodrigues Parameters," *Journal of the Astronautical Sciences*, Vol. 44, No. 1, Jan.–March 1996, pp. 1–19.

[30] Schaub, H., Robinett, R. D., and Junkins, J. L., "New Penalty Functions for Optimal Control Formulation for Spacecraft Attitude Control Problems," *Journal of Guidance, Control, and Dynamics*, Vol. 20, No. 3, May–June 1997, pp. 428–434. doi:10.2514/2.4093

[31] Sasaki, T., Shimomura, T., and Kanata, S., "Spacecraft Attitude Control with RWs via LPV Control Theory: Comparison of Two Different Methods in One Framework," *Transactions of the Japan Society for Aeronautical and Space Sciences, Aerospace Technology Japan*, Vol. 14, No. ists30, 2016, pp. Pd_15–Pd_20. doi:10.2322/tastj.14.Pd_15

[32] Boyd, S., Ghaoui, E. L., Feron, E., and Balakrishnan, V., *Linear Matrix Inequalities in System and Control Theory*, Vol. 15, Studies in Applied Mathematics, Univ. City Science Center, Philadelphia, PA, 1994, Chap. 3. doi:10.1137/1.9781611970777

[33] Chilali, M., and Gahinet, P., "$\mathcal{H}_\infty$ Design with Pole Placement Constraints: An LMI Approach," *IEEE Transactions on Automatic Control*, Vol. 41, No. 3, March 1996, pp. 358–367. doi:10.1109/9.486637

J. McMahon
Associate Editor